Phase-field models

Mathis Plapp

Physique de la Matière Condensée, École Polytechnique, CNRS, 91128 Palaiseau, France

Abstract

The transport-limited growth of crystals can create complex morphologies due to the occurence of morphological instabilities and subsequent evolution of the interfaces. The phase-field method has emerged as a compact and elegant mathematical tool for the modelling and numerical simulation of such phenomena. It is based on the evolution equations of out-of-equilibrium thermodynamics, which are derived from Ginzburg-Landau free energy functionals. Interfaces are represented implicitly by profiles of suitable order parameters. This chapter will first introduce some fundamentals underlying the construction of phase-field models, and then review several phase-field models for solidification as examples for the description of complex microstructure formation processes.

Keywords: modelling, microstructure, solidification, thermodynamics

1. Introduction

Crystal growth can generate a huge variety of different morphologies. A visit to a good minerals collection or the observation of frost and snowflakes in winter will motivate any curious spirit to ask the question by which set of fundamental mechanisms this wealth of shapes is created. There are also some practical reasons that call for a precise understanding of pattern formation in crystal growth: many man-made materials are crystalline, and their properties depend on their microstructure. Hence, which patterns form for given processing conditions is a question of both fundamental and practical interest.

Fundamentally, crystal growth can be divided in two stages: new material has to be transported to the surface of the growing crystal, and it has to find its place in the structure of the growing crystal. Which of these is the rate-limiting step depends on the structure of the crystal interface at the atomistic

scale. For crystals that have a microscopically rough interface (atoms can easily attach to and detach from the surface, microscopic fluctuations of the interface structure are large), growth is mainly controlled by bulk transport. This is generally the case for metals. In this case, morphological instabilities occur, simple growth shapes are unstable, and complex microstructures develop, such as dendrites (tree-like, branched structures). In contrast, for crystals whose interfaces are smooth on an atomic scale, growth is mainly controlled by the kinetics of incorporation, which depends on the density of surface defects such as steps, kinks, and dislocation outcrops. Generally, this growth mode leads to the emergence of strongly facetted shapes, such as found in many minerals.

Historically, the problem of transport-limited crystal growth was first formulated as a *free boundary problem* [1, 2]: the interface is represented by a mathematical surface without thickness, and its local growth velocity is proportional to the flux of heat and/or matter that arrives at the crystal surface. The temperature and concentrations at the surface obey thermodynamic boundary conditions, and fluxes of heat and matter follow the appropriate transport laws inside the volume of both phases. While this formulation is simple and intuitive, free boundary problems are known to be extremely hard to solve, both analytically and numerically.

Since about 30 years, the phase-field method has been established as a new approach to the modelling of transport-limited crystal growth. Surfaces and interfaces are described implicitly by one or several scalar fields, the so-called phase fields, that describe the local state of matter. The equations of motion for these fields are rooted in the physics of phase transitions and can be obtained from the laws of out-of-equilibrium thermodynamics. They are coupled to the transport equations for heat and chemical constituents. The advantage of the phase-field approach is that an explicit tracking of the evolving interfaces is avoided, which makes it possible to implement phase-field models with the standard mathematical methods used for any set of coupled partial differential equations. The phase-field method has been extremely successful in the description of crystal growth; in particular, it has had a tremendous impact on the understanding of solidification microstructures.

The phase-field method is also used in many other fields, such as for example solid-state phase transformations [3] and hydrodynamics [4], and has become one of the standard methods for the modelling of moving interfaces. Therefore, the available literature is abundant. There are several pedagogic reviews [5, 6, 7, 8], an introductory book [9], and several recent papers review

various applications in crystal growth and solidification [10, 11, 12, 13, 14]. Therefore, in the present contribution I will not attempt to be exhaustive, but instead present some essential concepts, "bricks" and ingredients that are needed to construct efficient phase-field models for crystal growth. Some of the material is fairly basic, but a thorough understanding of some fundamentals is necessary to appreciate the differences between the various models found in the literature, which are sometimes subtle but can have important consequences for the performance in simulations. One of the difficulties for a review of phase-field models is that the notations, conventions, and definitions are not standardized and differ between various "schools". Sometimes, I will attempt to quote several different formulations, but an exhaustive panorama would be too lengthy. I will restrict the presentation to phase-field models for solidification; it will be assumed in the following that the reader is familiar with the fundamentals of solidification science [15, 16, 17]. Phase-field models for step-flow growth during molecular beam epitaxy are briefly reviewed by W. Miller in chapter 12 of Vol. 1a of this book.

For the understanding of phase-field models, it is useful to take two complementary perspectives: a "bottom-up" and a "top-down" view. On the one hand, order-parameter models have originally been developed as a continuum description of phase transitions. They can therefore be obtained, by a coarse-graining procedure, from microscopic models (as described in section 2), which provides one of the centerpieces of phase-field models, namely, a mesoscopic free energy functional. This description naturally yields *diffuse interfaces*, some properties of which will be reviewed in section 3. On the other hand, phase-field models can be seen as a numerical tool for the solution of free-boundary problems; in this "top-down" perspective, the diffuse interfaces are a mathematical regularization of a sharp-interface problem (section 4). These two viewpoints are combined in section 5 to construct phase-field models for a variety of solidification phenomena. Finally, section 6 will present a brief conclusion and a selection of open problems.

2. Order-parameter models: the "bottom-up" view

The roots of the phase-field method can be found in the continuum description of phase transitions. A characteristic feature of first-order phase transitions is the coexistence of two thermodynamic phases. This implies the existence of interfaces that delimit the domains occupied by each phase. Seen on a macroscopic scale, these interfaces appear as surfaces of discontinu-

ity in an otherwise continuous medium. However, on the microscopic scale, interfaces have a finite width and an internal structure. The first theory for a phase transition with *diffuse interfaces* was formulated by van der Waals for the liquid-vapor transition in a one-component fluid (pure substance) [18]. Later on, this description was connected to the general theory of phase transitions by Ginzburg and Landau. The first application to materials science was the Cahn-Hilliard equation for the evolution of composition in binary mixtures [19].

In this approach, the spatial structure and time evolution of a heterogeneous system is described by a continuous field that is identified with a physical quantity – the *order parameter* of Landau theory. The time evolution of this field is then given by the laws of out-of-equilibrium thermodynamics, taking into account the nature of the order parameter (scalar, vector, or tensor), its conservation laws, and the symmetries of the problem.

In principle, the evolution equations can also be obtained directly from a microscopic description using the method of *coarse-graining*. While this procedure can in general not be carried out explicitly without drastic approximations, it provides insights into numerous properties of order-parameter models. Therefore, it seems useful to outline as an example the principal steps that need to be taken in order to obtain diffuse-interface equations for two simple lattice models, the Ising model for the ferromagnetic to paramagnetic transition and a binary lattice alloy model; more details can be found in [5].

In its simplest version, the microscopic Hamiltonian of the Ising model is given by

$$\mathcal{H} = -J \sum_{\langle i,j \rangle} S_i S_j - h \sum_i S_i. \tag{1}$$

Here, i and j denote points on a lattice, which for simplicity is assumed to have periodic boundary conditions and to be large enough for finite-size effects to be negligible. The "spin variables" (magnetic moments) S_i can take the values ± 1, the first sum runs over the pairs of nearest neighbor sites, and the constant J is positive, such that parallel alignment of neigboring spins is favoured. The second term describes the interaction of the spins with the external magnetic field h.

The thermodynamic (Helmholtz) free energy F is obtained from the standard formula

$$F = -k_B T \ln Z, \tag{2}$$

where k_B is Boltzmann's constant, T is the (fixed) temperature, and the partition function is given by

$$Z = \sum_{\mathcal{C}} \exp\left(-\frac{\mathcal{H}(\mathcal{C})}{k_B T}\right), \tag{3}$$

where the sum runs over all possible configurations $\mathcal{C}$, that is, all possible sets of spin values $\{S_i\}$.

With these definitions, F is a function of temperature T and magnetic field h. In order to describe inhomogeneous systems, some information about the spatial distribution of spin values needs to be retained. To this end, space is divided in "cells", say cubes of ℓ^d lattice sites, where d is the space dimension. Then, in each cell (labeled by capital indices), a local magnetization is defined by

$$m_I = \frac{1}{\ell^d} \sum_{i \in I} S_i. \tag{4}$$

The calculation of the partition function can now be split in two steps:

$$Z = \sum_{\{m_I\}} \sum_{\mathcal{C}/\{m_I\}} \exp\left(-\frac{\mathcal{H}(\mathcal{C})}{k_B T}\right). \tag{5}$$

The idea is that the same set of cell magnetizations can in general be obtained by many different microscopic configurations; the second sum in Eq. (5) runs over all the microstates that are compatible with the "imposed" set of cell magnetizations. A free energy can then be defined by the logarithm of just the second sum,

$$\mathcal{F}(\{m_I\}) = -k_B T \ln \sum_{\mathcal{C}/\{m_I\}} \exp\left(-\frac{\mathcal{H}(\mathcal{C})}{k_B T}\right). \tag{6}$$

This *mesoscopic* free energy depends on the set of m_I, and therefore on the spatial structure of the magnetization field. The thermodynamic free energy can then be obtained by summation over the cell variables, which corresponds to the outer sum in Eq. (5).

It is generally impossible to evaluate explicitly these formulas. To make further progress, the standard path is to use mean-field approximations for the coarse-grained free energy. The local magnetization variables are hence replaced by local average values. Furthermore, under the assumption that

the magnetization varies slowly on the scale of a coarse-graining cell, the magnetization values in the individual cells can be interpolated by a continuous magnetization field, and the first sum in Eq. (5) can be replaced by an integral. As a result, the coarse-grained free energy takes the Ginzburg-Landau form

$$\mathcal{F} = \int_V \left[\frac{1}{2} \tilde{K} \left(\nabla m \right)^2 + f(m) \right] \, dV, \tag{7}$$

where integration is over the volume of the system, $f(m)$ is the local free energy density (the free energy calculated for a single coarse-graining cell), and the gradient term arises from the interactions between neighboring coarse-graining cells (the constant $\tilde{K}$ is proportional to the interaction energy J and to the number of lattice bonds between neighboring cells). For the Ising model, the free energy density in the mean-field approximation takes the form

$$\begin{aligned} f(m) \;\; = \;\; & \frac{1}{a^d} \left\{ -\frac{zJ}{2} m^2 - hm \right. \\ & \left. + k_B T \left[\left(\frac{1+m}{2} \right) \ln \left(\frac{1+m}{2} \right) + \left(\frac{1-m}{2} \right) \ln \left(\frac{1-m}{2} \right) \right] \right\} \end{aligned} \tag{8}$$

where a is the lattice spacing and z the coordination number of the lattice (number of first neighbors). The first two terms inside the braces represent the spin-spin interactions and the interaction with the external magnetic field, respectively; the third term represents the contribution of the configurational entropy to the free energy. An expression that is easier to handle analytically is obtained by a Taylor expansion around the *critical point* ($T = T_c = zJ/k_B$, $m = 0$), which yields (up to a constant that can be omitted)

$$f(m) = \frac{1}{a^d} \left\{ \frac{1}{2} k_B (T - T_c) m^2 + \frac{1}{12} k_B T_c m^4 - hm \right\}. \tag{9}$$

This free energy density is plotted in Fig. 1 for temperatures above and below the critical temperature. For $T > T_c$, the system is *paramagnetic*: the free energy has a single minimum, the location of which is shifted by the application of a magnetic field. For $T < T_c$, $f(m)$ has a double-well structure. For zero magnetic field, the two minima are equivalent, which corresponds to the coexistence of two phases with opposite spontaneous magnetizations: the system is *ferromagnetic*. The transition from the paramagnetic to the

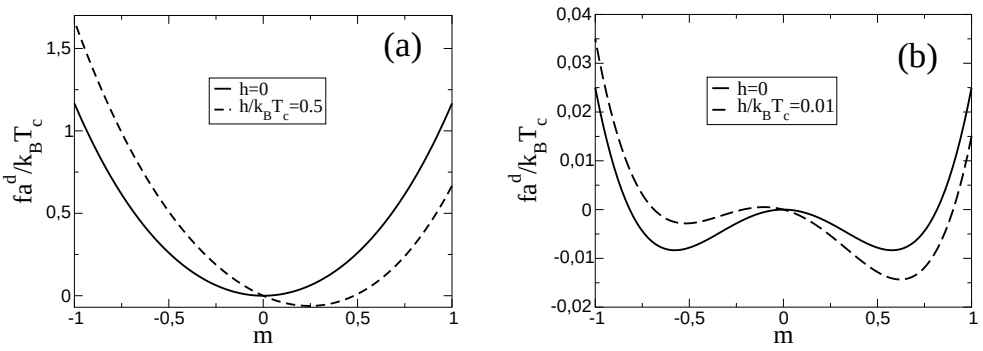

Figure 1: The free energy density given by Eq. (9) for (a) $T = 2\,T_c$ and (b) $T = 0.9\,T_c$.

ferromagnetic state is of second order (the equilibrium magnetization varies continuously with temperature). Below T_c, there is a first-order transition when the magnetic field is varied: the magnetization jumps discontinuously from one minimum to the other when the magnetic field crosses zero. For a range of magnetic fields around $h = 0$, there are still two minima, but with different values of the free energy density; the higher one of the two corresponds to a metastable phase.

There are several methods to obtain an equation of motion for this model. We will follow here standard arguments of irreversible thermodynamics. Equilibrium is reached when the total free energy is minimal; therefore, an equation which implies a decrease in the free energy will drive the system towards (global or local) equilibrium. The time derivative of the total free energy is

$$\frac{d\mathcal{F}}{dt} = \int_V \frac{\delta \mathcal{F}}{\delta m(\vec{x})} \frac{\partial m(\vec{x},t)}{\partial t}\, d\vec{x}, \tag{10}$$

where $\delta F/\delta m(\vec{x})$ denotes the functional derivative of the free energy functional with respect to the magnetization at the point $\vec{x}$, and we have used the chain rule for differentiation. It is easy to see that we always have $d\mathcal{F}/dt \leq 0$ if we choose

$$\frac{\partial m}{\partial t} = -\Gamma \frac{\delta \mathcal{F}}{\delta m(\vec{x})}, \tag{11}$$

where Γ is a positive constant: this expression makes the integrand on the right hand side of Eq. (10) negative or zero. The quantity $\delta\mathcal{F}/\delta m$, that is, the variation of the free energy with the local magnetization, can be interpreted as a thermodynamic force, and Γ as a mobility. The local magnetization is a non-conserved quantity, since it can change by simple flips of the spins inside

a coarse-graining cell. Equation (11) thus simply expresses that the rate of change of the magnetization is proportional to the thermodynamic driving force. It can be shown by statistical mechanics methods (linear response theory) that this proportionality is always valid for small enough driving forces and for systems in which the time evolution results from the superposition of numerous microscopic processes.

Let us now consider a binary lattice alloy model. Lattice sites are occupied by atoms A or B (no vacancies), and atoms interact only when they are on nearest neighbor sites, with atoms of the same kind contributing a negative energy. It can be shown through a simple change of variables that the microscopic Hamiltonian is then completely equivalent to the one of the Ising model, with "up spins" corresponding to A atoms, and "down spins" to B atoms. As a consequence, the coarse-grained free energy functional is also equivalent. It is usually written in terms of the composition, or local fraction of B atoms (the number of B atoms in a coarse graining cell divided by the number of lattice sites in the cell), which is related to the magnetization m by

$$c \leftrightarrow \frac{1-m}{2}. \tag{12}$$

The phase transition is now from a miscible to a phase-separated mixture: for $T > T_c$, the system is miscible (all compositions are stable). For $T < T_c$, a miscibility gap exists: for a range of composition, the system separates into an A-rich and a B-rich phase.

There is one decisive difference between the two systems: whereas the local magnetization can change by a simple flip of a spin, an A atom cannot transform into a B atom. The number of B atoms in a cell can therefore only change if atoms are exchanged between neigboring cells; the composition c obeys a *conservation law*:

$$\frac{\partial c}{\partial t} + \vec{\nabla} \cdot \vec{J} = 0, \tag{13}$$

where $\vec{J}$ is the exchange current of A and B atoms. Under this constraint, the time derivative of the free energy becomes

$$\frac{d\mathcal{F}}{dt} = \int_V \frac{\delta \mathcal{F}}{\delta c(\vec{x})} \frac{\partial c(\vec{x},t)}{\partial t}\, d\vec{x} = -\int_V \frac{\delta \mathcal{F}}{\delta c(\vec{x})} \vec{\nabla} \cdot \vec{J}\, d\vec{x}. \tag{14}$$

Integration by parts yields for a closed system (no mass currents through the

system boundaries)

$$\frac{d\mathcal{F}}{dt} = \int_V \vec{J} \cdot \vec{\nabla} \frac{\delta \mathcal{F}}{\delta c(\vec{x})} d\vec{x}. \tag{15}$$

A decrease in the free energy can thus be guaranteed by the choice

$$\vec{J} = -M \vec{\nabla} \frac{\delta \mathcal{F}}{\delta c(\vec{x})} = -M \vec{\nabla} \tilde{\mu}, \tag{16}$$

with M a positive constant. Again, this equation has a direct microscopic interpretation. The variation $\delta\mathcal{F}/\delta c$ (designated by $\tilde{\mu}$ in the second equality of the right hand side of Eq. (16)) is the change in free energy with composition; the system can therefore lower its energy if B atoms flow to regions where $\tilde{\mu}$ is lower, and A atoms in the opposite direction. The gradient of $\tilde{\mu}$ hence drives the mass currents that corresponds, on a microscopic level, to exchange processes between A and B atoms. The quantity $\tilde{\mu}$ is sometimes called "chemical potential", sometimes "diffusion potential"; it is given by

$$\tilde{\mu} = \rho(\mu_B - \mu_A), \tag{17}$$

where $\mu_i = \partial F / \partial N_i|_{T,V,N_j}$ are the "standard" chemical potentials of A and B atoms, and ρ is the density of lattice sites (in other words, $\rho = \mathcal{N}_A / V_m$, with $\mathcal{N}_A$ the Avogadro number and V_m the molar volume of the mixture). Equation (16) again is the product of a thermodynamic driving force (the gradient of diffusion potential) and a mobility M. The combination of Eqs. (13) and (16) yields the Cahn-Hilliard equation,

$$\frac{\partial c}{\partial t} = \vec{\nabla} \cdot \left[M \vec{\nabla} \frac{\delta F}{\delta c} \right]. \tag{18}$$

At this point, it is useful to make a number of general comments:

- We have obtained the evolution equations for the magnetization and the composition in the canonical ensemble (fixed temperature), with the free energy as the thermodynamic potential. The introduction of a Ginzburg-Landau free energy functional that has the form of an integral over a local free energy density implies the assumption that the individual coarse-graining cells are large enough to make the evaluation of local partition functions and statistical averages meaningful. In this case, the equivalence between statistical ensembles applies, and

the evolution equations can also be formulated in other thermodynamic ensembles. Many authors have started from an entropy functional (microcanonical ensemble, see for example [20]), and used the condition that the local entropy production must always be positive. Grand-canonical approaches have also been used more recently [21, 22, 23].

- The mobilities introduced in Eqs. (11) and (16) can depend on local state variables, on space and/or time, as long as they remain positive.

- We have obtained the evolution equations by thermodynamic arguments. It is also possible to derive them from microscopic models, which often makes it possible to obtain expressions for the mobility functions. Lattice models are very naturally simulated by the Monte Carlo method, which defines a microscopic stochastic process. The microscopic master equation can then be used to describe the evolution of local averages. In a kinetic mean-field approximation, it is possible to obtain evolution equations of the form of Eqs. (11) and (18) for simple spin-flip and particle-exchange models, respectively (see [24] for a review).

- The definition of a coarse-grained free energy functional implies the choice of a coarse-graining length (in the above example, the cell size ℓ). Obviously, the free energy density as well as the gradient energy coefficient $\tilde{K}$ depend on this choice, since the number of microscopic configurations inside a coarse-graining cell and the interaction strength between neighboring cells both depend on ℓ. This dependence on ℓ disappears in the mean-field approximation, but is present in more accurate evaluations of the partition functions, which is perfectly natural since the mesoscopic functional $\mathcal{F}$ can contain only the free energy of all fluctuations on length scales below ℓ. The complete free energy is obtained by the outer summation in Eq. (5). In the dynamic Eqs. (11) and (18), these large-scale fluctuation modes can be included by additional stochastic noise terms, which transforms them into Langevin equations. Indeed, it is clear that under a given microscopic dynamics (for example, a Monte Carlo process), the cell variables exhibit fluctuations with an amplitude that depends on the coarse-graining size. Therefore, the noise amplitude has to be consistent with the free energy functional. More detailed investigations of these questions in the context of solid-state diffusion can be found in Refs. [25, 26]. Some further

issues concerning the addition of noise are discussed in Refs. [22, 27].

- Whereas coarse-graining is conceptually simple and intuitive, it generally cannot be performed rigorously. It relies on strong assumptions about scale separation: on the one hand, the coarse-graining cells must be large enough to justify the use of local thermodynamic identities; on the other hand, the cells must remain small enough to be considered homogeneous, that is, they must remain smaller than the correlation length. For solid-liquid interfaces in metals, the typical width of the microscopically rough interface is about half a nanometer, which corresponds to only a few atomic distances [28]. Therefore, there exists no intermediate scale between the size of an atom and the thickness of the interface on which coarse-graining could be rigorously performed. In the vicinity of a critical point, where the correlation length diverges, the fluctuations also diverge such that mean-field approximations break down. Therefore, direct quantitative results for the thermodynamic description of specific systems cannot be expected from mesoscopic free-energy functionals, which should rather be seen as a phenomenological description.

- The Taylor expansion that leads from Eq. (8) to Eq. (9) is an example for a Landau expansion. The idea of Landau theory is that for *any* phase transition there exists a suitable order parameter that can distinguish between the different phases. Around a critical point, the free energy density can always be expanded in a polynomial form that only depends on the structure of the order parameter and the symmetries of the considered problem. First-order phase transitions can also be phenomenologically described by such free-energy densities, despite the fact that they may not exhibit a critical point. As a consequence, it is straightforward to write down order-parameter models for a large variety of phenomena: it is sufficient to identify the suitable order parameters and their conservation laws. The Landau expansion, together with gradient square terms, yields the free energy functional, and the conservation laws determine the form of the equations of motion. A classification of the simplest possible models was given by Hohenberg and Halperin [29]. In this list, Eq. (11) (one non-conserved order parameter) is called model A, Eq. (18) (one conserved order parameter) model B; model C has one non-conserved and one conserved order pa-

rameter and was the original starting point for phase-field models of solidification [30, 31, 32]; finally, a model that includes hydrodynamics is called model H. It describes the liquid-vapor transition of a one-component fluid, taking into account conservation of mass, momentum, and energy.

3. Diffuse interfaces at equilibrium

Two-phase coexistence implies the existence of interfaces. Their properties can readily be obtained from the Ginzburg-Landau free energy functional introduced in the preceding section. This will first be illustrated for the simple example of the Ising model, and then discussed in more generality.

Let us consider a ferromagnetic state of the Ising model ($T < T_c$) without magnetic field ($h = 0$). The local free energy density given by Eq. (9) has two minima for

$$f'(m) = 0 \qquad \leftrightarrow \qquad m = \pm m_{\rm eq} \qquad m_{\rm eq} = \sqrt{6\frac{(T_c - T)}{T_c}} \tag{19}$$

In terms of $\psi = m/m_{\rm eq}$, the free energy can be rewritten as

$$\mathcal{F} = \int \frac{1}{2} K \left(\vec{\nabla}\psi\right)^2 + H f_{\rm dw}(\psi), \tag{20}$$

with $K = \tilde{K} m_{\rm eq}^2/a^d$, $H = k_B T_c m_{\rm eq}^4/(3a^d)$ and the double-well function (with minima at $\psi = \pm 1$)

$$f_{\rm dw}(\psi) = -\frac{\psi^2}{2} + \frac{\psi^4}{4}. \tag{21}$$

In this formulation, all the physical parameters are contained in the two constants K and H. They have dimension of energy per unit length and energy per unit volume, respectively. From this, we can immediately deduce fundamental scaling relations for the thickness ξ of the interface (a length) and its surface free energy γ (energy per unit surface),

$$\xi \sim \sqrt{\frac{K}{H}}, \tag{22}$$

$$\gamma \sim \sqrt{KH} \sim H\xi. \tag{23}$$

To understand these relations, observe that the first term in the integral of Eq. (20) is minimized by a flat profile (with zero gradients), whereas

the second one favors values of ϕ close to ± 1 and is thus minimized by a step function. Therefore, the finite interface thickness results from the competition between the two terms in the functional. Moreover, inside the interface, the field ψ takes values in between the two minima, such that the interface contributes an extra free energy density of order H (from the "potential" $Hf_{\rm dw}$) across a space region of thickness ξ.

For a more rigorous derivation of these relations, consider the equation for an equilibrium interface, $\delta F/\delta\psi = 0$, for a planar interface oriented normal to the x direction, with a profile $\psi(x)$. The evalution of the functional derivative (see Eq. (60) below for the precise definition of this procedure) yields

$$-K\partial_{xx}\psi + Hf'_{\rm dw}(\psi) = 0, \tag{24}$$

where $\partial_{xx}\psi$ is shorthand for $\partial^2\psi/\partial x^2$, and $f'_{\rm dw}$ denotes the derivative of $f_{\rm dw}$ with respect to ψ. We introduce the dimensionless coordinate $\tilde{x} = x/W$ with $W = \sqrt{K/H}$. After a change of variables from x to $\tilde{x}$ and division by H, Eq. (24) becomes

$$-\partial_{\tilde{x}\tilde{x}}\psi + f'_{\rm dw}(\psi) = 0. \tag{25}$$

Therefore, the interface profile $\psi_{\rm eq}(\tilde{x})$ is determined by the the double-well function; only its length scale depends on the physical parameters.

Far away from the interface, the magnetization tends to its equilibrium values $m = \pm m_{\rm eq}$ ($\psi = \pm 1$), and the bulk free energy density is $Hf_{\rm dw}(\pm 1)$. For definiteness, let us suppose that $\psi(-\infty) = 1$ and $\psi(\infty) = -1$. The surface energy γ is defined as the excess free energy (per surface area) due to the presence of an interface. This can be expressed as

$$\begin{aligned}\gamma &= \int_{-\infty}^{\infty}\left\{\frac{1}{2}K(\partial_x\phi)^2 + H\left[f_{\rm dw}(\psi(x)) - f_{\rm dw}(\pm 1)\right]\right\}\,dx \\ &= \sqrt{KH}\int_{-\infty}^{\infty}\left\{\frac{1}{2}(\partial_{\tilde{x}}\phi)^2 + \left[f_{\rm dw}(\psi(x)) - f_{\rm dw}(\pm 1)\right]\right\}\,d\tilde{x}.\end{aligned} \tag{26}$$

This integral can be simplified with the help of a relation that is obtained from Eq. (25) by multiplying both sides with $\partial_{\tilde{x}}\psi$ and integrating from $-\infty$ to $\tilde{x}$, which yields

$$\frac{1}{2}\left(\partial_{\tilde{x}}\psi\right)^2 = f_{\rm dw}(\psi(\tilde{x})) - f_{\rm dw}(\pm 1). \tag{27}$$

This result can be used to eliminate either one of the two terms in the integral of Eq. (26); after the elimination of the square gradient term and a change

of integration variable from $\tilde{x}$ to ψ, γ can be evaluated as

$$\gamma = \sqrt{KH} \int_{-1}^{1} \sqrt{2\left[f_{\mathrm{dw}}(\psi) - f_{\mathrm{dw}}(\pm 1)\right]}\, d\psi = \sqrt{KH}I \tag{28}$$

where I (the value of the integral) is defined by the second equality. For the fourth-order polynomial given by Eq. (21), $I = 2\sqrt{2}/3$, and the interface solution is given by

$$\psi(x) = -\tanh\left(\frac{x - x_0}{\sqrt{2}W}\right) \tag{29}$$

for an interface centered at x_0.

Again, several general remarks can be made:

- The fourth-order polynomial given by Eq. (21) is the most popular choice for a double-well function, both because it is the lowest-order double-well function that appears in a Landau expansion and because of the existence of a closed-form analytic solution for the interface. However, any other double-well function yields a similar interface shape (that is, a sigmoid curve) because of Eq. (25): the modulus of the slope is highest in the center of the interface, where ψ is "on the top" of the potential barrier.

- The definition of the interface thickness ξ is somewhat arbitrary, and many different conventions have been used in the literature. One choice that works for arbitrary potentials is to define ξ as the inverse of the maximum slope, $\xi = 1/\max(|\partial\psi/\partial x|)$, which yields $\xi = \sqrt{2}W$ for the fourth-order polynomial.

- The above results can be used to rewrite the free energy in two different forms, which both have been used in the literature. In the first, the coefficient H of the double-well potential is pulled out of the integral, and the definition $W^2 = K/H$ is used to obtain [33]

$$\mathcal{F} = H \int_V \frac{1}{2} W^2 \left(\vec{\nabla}\psi\right)^2 + f_{\mathrm{dw}}(\psi). \tag{30}$$

  The ratio $\mathcal{F}/H$ is sometimes called "dimensionless free energy", although it is the free energy *density* (the integrand) which is dimensionless. Therefore, when the prefactor H is absorbed in the definition of $\mathcal{F}$, the latter acquires the dimension of a volume, and the surface free

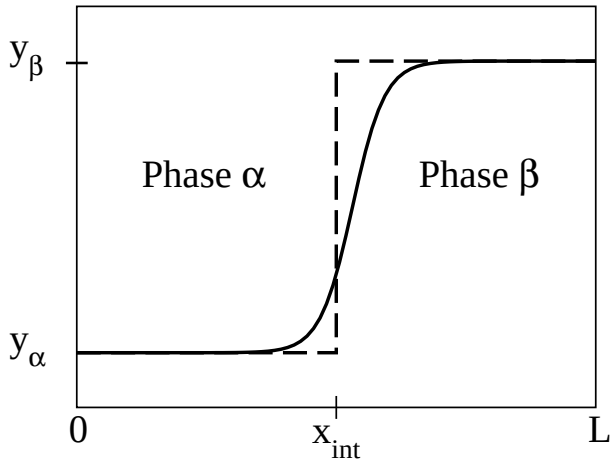

Figure 2: Illustration of the Gibbs construction: thermodynamic properties and a position on a macroscopic scale can be assigned to a diffuse interface by comparing the total content of an extensive quantity $y(x)$ with the one of a step function, localized at the position $x_{\rm int}$, between the macroscopic values of y in the two phases.

energy becomes a length [33]. The advantage of this convention is that a rescaling of all lengths by W yields equations that do not contain any coefficients, such as Eq. (25). Another possibility to rewrite the free energy is to eliminate the coefficients K and H in the functional in favor of ξ and γ. The result for the fourth-order polynomial is

$$\mathcal{F} = \int_V \frac{3}{8}\gamma \left[\xi \left(\vec{\nabla}\psi \right)^2 + \frac{f_{\rm dw}(\psi)}{\xi} \right]; \tag{31}$$

both the square gradient and the potential term have to be modified if the interface thickness is to be changed at constant surface energy.

Let us now generalize these results for other interfaces. Consider a mixture of K different components in which two phases are in coexistence (elastic effects are not included here for simplicity; for a detailed discussion of stress effects on interface thermodyamics, see for example [34]). The extensive thermodynamic quantities are energy E, entropy S, and the number N_i of particles of species i, with volume densities e, s, and ρ_i, respectively. The conjugate intensive variables for S and N_i are the temperature T and the chemical potentials μ_i. Since there is an equilibrium between two phases which can exchange energy and particles, all the intensive variables must be equal in the two phases, and uniform in inhomogeneous systems (and, thus,

in diffuse interfaces). In contrast, the densities of the extensive quantities can be different in the two phases, and vary through the interface region in a continuous manner, like in the example of the magnetization seen above. Macroscopic thermodynamic properties can be assigned to such profiles through the classic Gibbs construction, illustrated in Fig.2: in a system of total lengh L that contains an interface normal to the x direction, the total amount of an extensive quantity of density $y(x)$ is compared to a macroscopic two-phase system with an interface at position $x_{\rm int}$, and the difference is assigned to the interface,

$$y_{\rm int} = \left[\int_0^L y(x)\, dx\right] - \left[y_\alpha x_{\rm int} + y_\beta (L - x_{\rm int})\right], \tag{32}$$

where y_α and y_β are the bulk densities of y in the two phases. If $y_\alpha \neq y_\beta$, the value of the interface excess depends on the choice of the interface position $x_{\rm int}$. Therefore, it is always possible to *define* the interface position such that the interface excess is zero. However, when several extensive quantities exhibit variations through the interface, only one of the corresponding excess quantities can be made zero by the choice of the interface position, except in the presence of special symmetries.

The interface free energy is the interface excess of the relevant thermodynamic potential, which is often quite loosely called "free energy" without further precisions. "Relevant" means that this potential must have the same value in the two phases; otherwise, the surface energy cannot be defined unambiguously since it would depend on the choice of the interface position. Since the coarse-grained description is based on volume integrals, we will consider a system of fixed total volume V. In that case, the relevant potential is the grand potential. In contrast, if a fixed pressure is assumed, the relevant potential is the Gibbs free energy. See [35] for a detailed discussion on how to define interface excesses in this case. For constant volume, the pressure is not an independent variable, but is equal to the negative of the grand potential density, $-P = e - Ts - \sum_{i=1}^{K} \mu_i \rho_i$. The equality of the pressures in the two phases therefore implies

$$e_\alpha - Ts_\alpha - \sum_i \mu_i \rho_i^\alpha = e_\beta - Ts_\beta - \sum_i \mu_i \rho_i^\beta, \tag{33}$$

where ρ_i^ν are the equilibrium number densities of component i in phase ν.

Two special cases merit further discussion. For a pure substance ($K = 1$) in which both phases have equal number densities ($\rho_\alpha = \rho_\beta$), Eq. (33) reduces

to $e_\alpha - Ts_\alpha = e_\beta - Ts_\beta$, that is, $f_\alpha = f_\beta$, with the free energy densities $f_\nu = e_\nu - Ts_\nu$. Therefore, the surface free energy is given by the excess of the Helmholtz free energy. Note that we have already used this fact in the definition of γ for the magnetic model, Eq. (26), in which the two phases are related by the up-down symmetry of the spins. For a binary mixture ($K = 2$) of A and B particles with constant number density (or, equivalently, constant molar volume), $\rho_A + \rho_B = \rho$, $f_\alpha - (\mu_B - \mu_A)\rho_B^\alpha = f_\beta - (\mu_B - \mu_A)\rho_B^\beta$. Using that the composition $c = \rho_B/\rho = \rho_B V_a$, with $V_a = V_m/\mathcal{N}_A$ the volume occupied by an atom, we find

$$f_\alpha - \tilde{\mu} c_\alpha = f_\beta - \tilde{\mu} c_\beta = \omega_{\text{eq}}, \tag{34}$$

where $\tilde{\mu} = (\mu_B - \mu_A)/V_a$ is the diffusion potential introduced in Eq. (16). The surface free energy is the interface excess of $\omega = f - \tilde{\mu} c$ with respect to its equilibrium value ω_{eq},

$$\gamma = \int_{-\infty}^{\infty} \left[f - \tilde{\mu} c - \omega_{\text{eq}} \right] \, dx. \tag{35}$$

Let us now introduce the *phase field*. This name was coined in the beginning of the 1980s when the first diffuse-interface models for solidification were formulated [30, 31, 32]. The phase field is a scalar field that specifies the state of matter (solid or liquid). One may ask why such a field is needed, although the thermodyanmics of *any* system can be expressed in the traditional thermodynamic variables e, s, and ρ_i; indeed, the solid and liquid phases generally have different values for all of these quantities. Why not choose one of them as a marker to distinguish between solid and liquid ? The answer to this question lies in the particular nature of the solid-liquid transition, which does not have a critical point, contrary to the other phase transitions that have been discussed so far. Indeed, for a phase-separating mixture, there are two distinct phases at low temperature, which means that not all values of the composition are accessible; however, at high temperature the system becomes completely miscible. This means that there is a unique free energy function $f(c, T)$ which can describe all possible states of the system. The same holds for the liquid-gas transition and its free energy $f(\rho, T)$. For the solid-liquid transition, there is no continuous thermodynamic path that connects solid and liquid, which means that these two phases must be described by separate free energy curves. Therefore, an additional parameter is needed to interpolate between these curves.

A physical interpretation can be given to the phase field as the order parameter of the solid-liquid transition, which can be defined even if there is no critical point for this transition. A pure solid and its liquid are distinguished by the long-range order present in the crystal, which can be probed by diffraction experiments. Order parameter functions can be defined that locally detect crystalline order in the data of molecular dynamics simulations [36, 37]. In classical density functional theory, the fundamental field is the probability of presence of an atom at a particular position. Whereas this probability density is uniform in a liquid, for a solid it exhibits peaks around the equilibrium positions of the atoms in the lattice. This means that in reciprocal space the amplitude of certain "density waves" is finite for a solid, but zero for a liquid. Therefore, the amplitudes of density waves can be used as order parameters [38]. If this amplitude is allowed to vary in space on a scale much larger than the lattice spacing, in the spirit of amplitude equations, the free energy for solid-liquid coexistence takes a Ginzburg-Landau form, with a double-well potential and square gradient terms for the amplitude [39]. Therefore, the assumption of a Ginzburg-Landau form for the contribution of the phase field to the free energy is well justified.

The phase field ϕ is usually defined as the normalized order parameter, that is, $\phi = 0$ in the liquid and $\phi = 1$ in the solid. All the formulas derived so far for the dimensionless magnetization field ψ are also valid for the phase field, with the change of variables $\phi = (1 + \psi)/2$; the standard double-well potential used for ϕ is $f_{\mathrm{dw}} = \phi^2(1 - \phi)^2$. The phase field ϕ exhibits a variation through the interface, just like the extensive thermodynamic quantities. However, there is no intensive variable that is conjugate to the phase field. The phase field can be related to the volume fraction of solid: in a system of volume V, the latter is given by $(1/V) \int_V \phi(\vec{x})$, and a time evolution of the phase field corresponds to a relaxation of the volume fraction of solid towards its equilibrium value. Since the crystalline order can change locally by short-range motion of the atoms into or out of the equilibrium positions in a crystal lattice, the phase field is a non-conserved quantity and therefore must satisfy an equation of the type of Eq. (11). However, the evolution of the phase field (interpreted as a volume fraction) depends on the values of the local thermodynamic state variables, and therefore the equations for ϕ, the temperature and the composition are intrinsically coupled, as will be detailed below.

4. Free-boundary problems: the "top-down" view

In section 2, we have seen how mesoscopic free-energy functionals and equations of motion for the associated order parameters can be obtained by coarse-graining, that is, by averaging over the small length and time scales of the microscopic dynamics. Now we will take the opposite, "top-down" view and see how phase-field models can be obtained by introducing supplementary small scales into a macroscopic problem.

The starting point are *free-boundary problems*, introduced by Stefan [1, 2] for the growth of ice layers at a water surface in contact with cold air. In free-boundary problems, partial differential equations (usually for transport phenomena) need to be solved in domains that evolve with time in response to the fluxes at the boundaries. The time evolution of the domain boundaries is thus a part of the problem solution.

As a simple example, let us consider the freezing of a pure substance (the growth of a one-component pure crystal from its melt). We suppose that the density of solid and liquid are equal and that the melt is quiescent, such that no hydrodynamic flow needs to be taken into account. Under these circumstances, crystal growth is limited by the diffusion of heat: upon solidification, the latent heat is set free and has to be evacuated for crystal growth to continue. This problem can be formulated as a set of equations for the temperature field $T(\vec{x}, t)$ defined on domains of solid and liquid that are separated by a sharp interface:

$$\frac{\partial T}{\partial t} = D_\nu \vec{\nabla}^2 T \qquad (\nu = l, s) \tag{36}$$

$$V_n L = \hat{n} \cdot \left[C_s D_s \left. \vec{\nabla} T \right|_s - C_l D_l \left. \vec{\nabla} T \right|_l \right] \tag{37}$$

$$T_{\text{int}} = T_m - \frac{\gamma T_m}{L} \mathcal{K} - \frac{V_n}{\mu_k}. \tag{38}$$

The first equation describes the diffusion of heat in the two phases (liquid and solid), with D_s and D_l the associated heat diffusion coefficients. The second equation (Stefan condition) expresses the conservation of energy at the interface that advances with normal velocity V_n; L is the latent heat per unit volume, $\hat{n}$ the unit normal vector to the interface pointing into the liquid, and C_s and C_l the specific heats per unit volume in solid and liquid. Finally, Eq. (38) gives the boundary condition for the temperature at the

interface, which differs from the bulk melting temperature T_m by the Gibbs-Thomson effect (capillary shift of the melting temperature), where $\mathcal{K}$ is the interface curvature, and by interface dissipation due to the finite time of attachment of new atoms to the surface, with μ_k being the interface mobility (for more details, see for example [17]). Equation (38) also implies that the temperature is continuous at the interface.

For future reference, let us re-state this set of equations in terms of a dimensionless temperature field

$$u = \frac{T - T_m}{L/C_l}. \tag{39}$$

The equations (36) through (38) become

$$\frac{\partial u}{\partial t} = D_\nu \vec{\nabla}^2 u \qquad (\nu = l, s) \tag{40}$$

$$V_n = \hat{n} \cdot \left[(C_s/C_l) D_s \left.\vec{\nabla} u\right|_s - D_l \left.\vec{\nabla} u\right|_l \right] \tag{41}$$

$$u_{\text{int}} = -d_0 \mathcal{K} - \beta V_n. \tag{42}$$

Here, $d_0 = \gamma T_m C_l / L^2$ is the thermal capillary length and $\beta = C_l/(\mu_k L)$ is the kinetic coefficient. A particularly simple case that has been widely employed is the *symmetric model*, in which $C_s = C_l$ and $D_s = D_l$ are assumed.

The free-boundary formulation is appealing because it directly corresponds to our intuition about the motion of macroscopic domains – the finite thickness of the interfaces is hidden from our eyes or even the standard means of observation (for example, optical microscopes). Of course, this very fact is also the reason why sharp-interface models are an excellent description: there is a scale separation of several orders of magnitude between the thickness of the interface and the characteristic length scales of the macroscopic problem, such that the internal structure of the interfaces has no detectable effect on the macroscopic evolution.

However, free-boundary problems are notoriously difficult to solve. In *front tracking methods*, the interface is represented explicitly, for example by marker points that are located on the interface (Fig. 3). Boundary conditions and fluxes are then evaluated at this boundary, and the velocity of the points is computed. Problems arise, however, if the length of the interface increases (by ramification, for example) or if topological changes such as pinchoff or coalescence occur, because the interfaces need to be frequently re-meshed in

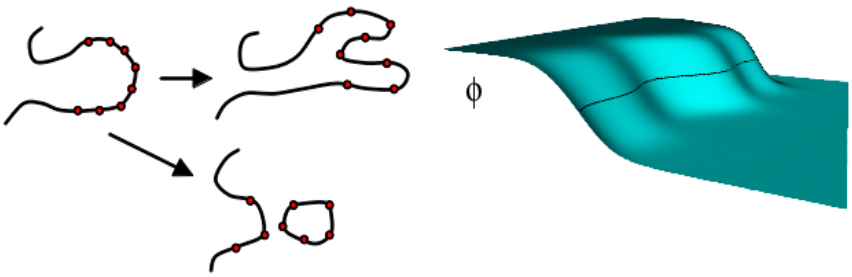

Figure 3: Illustration of interface tracking versus interface capturing methods: in interface tracking (left), the interface is represented *explicitly*, for example by marker points. In interface capturing (right), it is treated *implicitly* as a level set of a function that evolves with time (black line on the blue surface).

order to maintain a desired precision. The alternative idea of *front capturing methods* is to use an additional scalar field to implicitly represent the interface by one of its level sets. Since the level set changes when the field evolves, the laws of motion for the interface need to be translated into an evolution equation for the new field that takes into account the correct boundary conditions. The most well-known method of this type is probably the level-set method [40]. The phase-field method can be seen as another member of this family, with the additional advantage that its thermodynamic construction implies that number of boundary conditions at the interface, as well as the important conservation laws, are "automatically" incorporated. In this perspective, the phase field is seen as a mathematical tool for the computation of the interface evolution, and its equation of motion only needs to reproduce, on a large scale, the desired free-boundary problem.

Mathematically, this view of the phase field corresponds to a *regularization* of the free-boundary problem. Indeed, Eqs. (36) to (38) implicitly contain singularities: the materials properties (specific heat, diffusion coefficient) exhibit jumps at the interface, and the latent heat is released at the infinitely thin interface, which corresponds to a singular heat source term. Formally, this can be made apparent by rewriting Eqs. (40) to (42) in terms of distributions: the domain occupied by the solid is represented by an indicator function, $\theta_s(\vec{x})$, which equals 1 inside the solid, and zero outside. The interface location can then be described by a Dirac δ function that is related to the derivative of θ_s, $\vec{\nabla}\theta_s = -\delta(\vec{x} - \vec{x}_{\text{int}})\hat{n}$, where $\hat{n}$ is again the unit normal to the interface pointing into the liquid, and $\vec{x}_{\text{int}}$ is any point located

on the interface. Detailed discussions about this procedure can be found in [41, 42, 43, 44, 17].

The numerical treatment can be simplified by smoothing out these singularities. The smoothed indicator function of the solid domain can directly be identified with the phase field. In this spirit, the thickness of the smooth interfaces is not linked to any physical quantity, but is a mathematical parameter that can be freely chosen as long as the necessary scale separation is maintained. As a simple example, re-consider Eq. (31) for the surface free energy wth ξ as a free parameter. It can be seen, on the one hand, that in the limit $\xi \to 0$ the free energy excess is concentrated in an infinitely thin layer (while keeping a constant value), which corresponds to the sharp-interface formulation. On the other hand, an interface with a given free energy can be represented by a profile of arbitrary thickness ξ if the two terms in the interfacial free energy density are properly rescaled, as expressed by Eq. (31).

The smoothing of a sharp interface as described by Eq. (31) is exact for a stationary planar interface. When the interface is curved and/or in motion, the smoothing (which corresponds to the introduction of the additional length scale ξ) induces errors with respect to the original free boundary problem, which need to be quantified if the method is to be used as a reliable simulation tool. This can be accomplished by the method of *matched asymptotic expansions*, often also called boundary-layer calculations. The main steps of such a formal calculation are the following.

1. Define two different coordinate systems. The first one corresponds to the sharp-interface problem ("outer scale"), characterized by a macroscopic scale l specific to the considered problem (for example, the tip radius of in the case of dendritic growth). The second ("inner scale") is attached to the interface, and scaled by the interface thickness ξ. The ratio $\epsilon = \xi/l$ defines a small parameter.
2. Expand formally the relevant fields as a power series in the parameter ϵ on the two different scales, which gives an outer expansion and an inner expansion.
3. Solve the equations of the phase-field model perturbatively order by order in ϵ in each region, using the relevant coordinate system.
4. Match the two expansions order by order using the condition that the limit of the inner expansion far from the interface must coincide with the limit of the outer expansion when the interface is approached.
5. The result of this procedure are boundary conditions for the relevant

fields on the outer scale which are determined by the equations on the inner scale. In general, these boundary conditions also take the form of a power series in ϵ.

The explicit calculation of the matched asymptotics is quite tedious and has been presented in detail in several publications [33, 45, 46, 8]. Therefore, here only an example for a particular model will be reviewed: the celebrated phase-field model of Karma and Rappel [33]. It consists of two coupled equations for a phase field ψ that varies between $+1$ (solid) and -1 (liquid) and the dimensionless temperature field u defined in Eq. (39),

$$\partial_t \psi = W^2 \vec{\nabla}^2 \psi + \psi - \psi^3 - \lambda u (1 - \psi^2)^2, \tag{43}$$

$$\partial_t u = D \vec{\nabla}^2 u + \frac{1}{2} \partial_t \psi. \tag{44}$$

Here, W is the interface thickness as introduced in Eq. (30), and λ is a dimensionless constant. Details about the derivation of this model will be given in Sec. 5 below. In order to illustrate the procedure of asymptotic matching, we consider a planar interface of a solid that grows towards the positive x direction into a melt of initial dimensionless temperature $u(\infty) = -1 - \Delta$ with $0 < \Delta \ll 1$. It is easy to verify that the free-boundary problem has a steady-state solution: an interface propagating with a constant velocity $V = \beta\Delta$ and the temperature given by $u = -\Delta$ for $x < x_{\rm int}$ and $u = -1 - \Delta + \exp[-(x - x_{\rm int})V/D)]$ for $x > x_{\rm int}$. The numerical solution of the phase-field model given by Eqs. (43) and (44) is plotted in Fig. 4 on the two relevant scales. On the outer scale (given by the diffusion length $l = D/V$), the phase-field profile appears as a sharp step, and the slope of the temperature field has an apparent dscontinuity at the interface, as prescribed by the Stefan condition, Eq. (41). On the inner scale W, the slope of the temperature field changes slowly and continuously, since the source of latent heat is not concentrated in a single point, but "smeared out" over the entire interface region.

The two dash-dotted lines in Fig. 4b are fits to the asymptotes of the inner solution far from the interface, extrapolated to the interface position (the point where $\phi = 0$). This is an illustration of the matching condition between inner and outer fields: the boundary conditions for the field u "seen" on the outer scale correspond to the values of these asymptotes at the interface. Note that (i) the two asymptotes reach the same value at the interface position, so that the temperature is continuous on the outer scale, and (ii) that the value

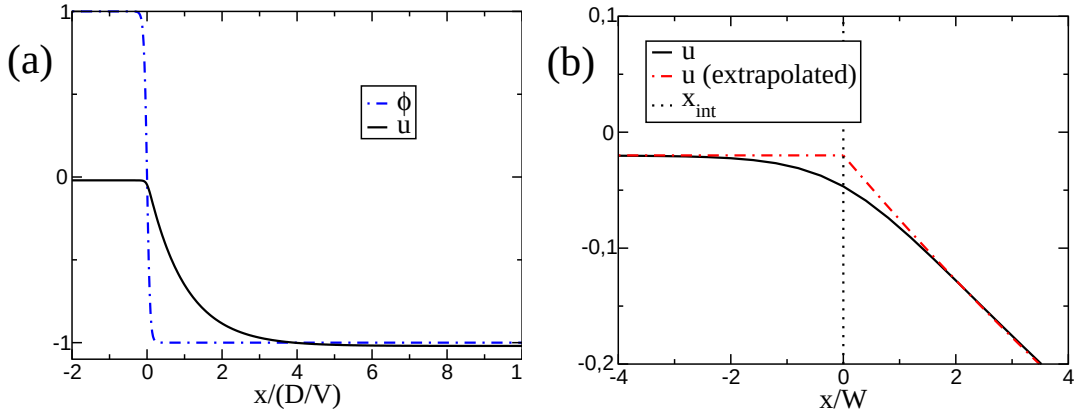

Figure 4: Steady-state solution of Eqs. (43) and (44) for $\Delta = 0.02$ and $\lambda = 1$, plotted on the scale of the diffusion length $l = D/V$ in (a) and on the scale of the interface thickness W in (b).

of u at the intersection point (that is, the boundary condition on the outer scale) does not correspond to any value of the actual field u taken inside the interface.

The main result of the asymptotic calculations is that the system of Eqs. (43) and (44) is equivalent to the symmetric model of solidification, with

$$d_0 = a_1 \frac{W}{\lambda} \tag{45}$$

$$\beta = a_1 \left[\frac{\tau}{\lambda W} - a_2 \frac{W}{D} \right], \tag{46}$$

where $a_1 = 5\sqrt{2}/8$ and $a_2 = 0.6267$ are numbers of order unity. The first of these equations describes the Gibbs-Thomson effect, and is "naturally" built into the phase-field model, as will be described below. The second deserves some more comments.

Equation (46) contains two terms. The first one is obtained if the temperature field is assumed to be constant inside the interface, and describes the dissipation due to a homogeneous undercooling of the interface. The second term is due to the inhomogeneities of the temperature field inside the interface, which are illustrated in Fig. 4b. After what has been said above, it may seem surprising that this contribution plays an important role: the characteristic scale for the variations of the temperature field is the diffusion length, and therefore an inhomogeneity on the scale of the interface should

be unimportant if WV/D is small enough. However, this reasoning neglects the heat source term in Eq. (44): this term varies on the scale of W and thus always creates contributions to the diffusion field on that scale; therefore, the second term of Eq. (46) is important even for small velocities [33].

The expression of the kinetic coefficient given by Eq. (46) is of crucial importance. Since there are two contributions of opposite sign, it is possible to choose $\beta = 0$, that is, to simulate interfaces in local equilibrium, with arbitrary interface thickness. The choice is limited, of course, by the convergence of the asymptotic matching procedure, which requires a sufficient separation between inner and outer scales. In practice, good convergence can often be obtained even with a scale ratio as large as 0.1. In order to appreciate the gain in computational time that can be achieved by this procedure, it is sufficient to remark that the smallest grid spacing needed to resolve a diffuse-interface model is proportional to the interface thickness. Therefore, being able to "upscale" the interface thickness with respect to its physically realistic value permits the use of larger grid spacings, and therefore also of larger timesteps. For a simple explicit algorithm on a regular grid, the number of numerical operations scales as $1/W^{d+2}$ [33], and thus an increase of the interface thickness by a factor of 100 provides a gain of 10^{10} in the computation time in three dimensions ($d = 3$) !

5. Phase-field models for solidification

The construction of a few elementary phase-field models for solidification will now be reviewed. In this exposition, the "bottom-up" and thermodynamic viewpoint is taken as a guideline, but repeated use of the "top-down" philosophy is also made in order to obtain efficient models that can be used to calculate solidification microstructures for realistic parameters.

5.1. Pure substance

Microstructure formation in a pure substance is mainly of academic interest. The growth of a dendritic monocrystal is a paradigmatic problem of pattern formation and has attracted an enormous amount of attention over many decades. It comes therefore as no surprise that this was also one of the first testbeds for the accuracy of phase-field models.

Let us consider the symmetric model of solidification, introduced in section 4, and choose the free energy as the thermodynamic potential (canonical

ensemble). The free energy functional is written in terms of a phase field ϕ that takes the values $\phi = 1$ in the solid and $\phi = 0$ in the liquid as

$$\mathcal{F} = \int_V f_{\rm int}(\phi, \vec{\nabla}\phi) + g(\phi) f_s(T) + (1 - g(\phi)) f_l(T). \tag{47}$$

Here, $f_{\rm int}$ represents the surface energy contribution and is of the form of Eq. (20), with $f_{\rm dw} = \phi^2(1-\phi)^2$, $f_s(T)$ and $f_l(T)$ are the free energy densities of solid and liquid, respectively, and $g(\phi)$ is an interpolation function that satisfies

$$g(0) = 0 \qquad g(1) = 1 \qquad g'(0) = g'(1) = 0. \tag{48}$$

The two choices that are most frequently used in the literature are the polynomials $g(\phi) = 3\phi^2 - 2\phi^3$ and $g(\phi) = 10\phi^3 - 15\phi^4 + 6\phi^5$. The motivation for Eq. (47) is easily understood: both of the quoted expressions for $g(\phi)$ are monotonous in ϕ, and therefore $g(\phi(\vec{x}))$ is an approximation for the step function $\theta_s(\vec{x})$, and $g(\phi)f_s(T) + (1 - g(\phi))f_l(T)$ approximates the bulk free energy in the sharp-interface formulation. Moreover, the first term, when integrated across the interface, yields the surface free energy, so that the volume integral of $f_{\rm int}$ is an approximation of the surface tension times the interfacial area.

The last condition in Eq. (48), $g'(0) = g'(1) = 0$, ensures that the bulk equilibrium values of the phase field are always equal to 0 or 1. Indeed, the phase field follows a non-conserved equation with mobility Γ,

$$\frac{1}{\Gamma}\partial_t\phi = -\frac{\delta\mathcal{F}}{\delta\phi} = K\vec{\nabla}^2\phi - H f'_{\rm dw}(\phi) - g'(\phi)\left[f_s(T) - f_l(T)\right]. \tag{49}$$

For a homogeneous system ($\vec{\nabla}\phi = 0$), since $g'(0) = g'(1) = 0$, the two fixed points of this equation are $\phi = 0$ and $\phi = 1$, even when $T \neq T_m$ and thus $f_s \neq f_l$.

The equation for the temperature can be obtained with the help of thermodynamic identities. First, we exploit the fact that the variation of the free energy with respect to the temperature is the opposite of the entropy density,

$$\frac{\delta\mathcal{F}}{\delta T} = -s(T,\phi) = -s_s(T)g(\phi) - s_l(T)[1 - g(\phi)], \tag{50}$$

where $s_\nu = \partial f_\nu(T)/\partial T$ are the entropy densities of liquid and solid. Next, we use that at constant density $de = Tds$, and find

$$de = T\frac{\partial s}{\partial T}dT + T\frac{\partial s}{\partial \phi}d\phi \tag{51}$$

with the help of the chain rule. Finally, we divide this equation by dt, combine it with the conservaton law for the internal energy density,

$$\partial_t e = \vec{\nabla}\left(CD\vec{\nabla}T\right), \tag{52}$$

and use that the specific heat $C = T\partial s/\partial T$ and the latent heat $L = T[s_l(T) - s_s(T)]$. The result is

$$C(\phi,T)\partial_t T = \vec{\nabla}(C(\phi,T)D\vec{\nabla}T) + Lg'(\phi)\partial_t\phi. \tag{53}$$

In the case of the symmetric model, C is independent of ϕ. Since, in addition we are interested in a limited range of temperatures around the melting point, we may approximate the values of C, s_s, s_l, and L by their values at the melting point. Then, we obtain the simple equation,

$$\partial_t T = \vec{\nabla}(D\vec{\nabla}T) + \frac{L}{C}g'(\phi)\partial_t\phi, \tag{54}$$

which is very intuitive: the temperature changes by heat diffusion in the bulk, and by the release of latent heat at the interface. The equation for the phase field can also be simplified by expanding the free energies in the right hand side around the melting temperature, which yields

$$\frac{1}{\Gamma}\partial_t\phi = K\vec{\nabla}^2\phi - Hf'_{\rm dw}(\phi) - g'(\phi)\frac{L}{T_m}(T - T_m). \tag{55}$$

The model of Karma and Rappel can now be obtained from these equations by the followng steps:

1. Choose the fifth-order polynomial for $g(\phi)$ and the standard fourth-order polynomial for $f_{\rm dw}$.
2. Replace the function $g(\phi)$ by another function $h(\phi)$ in the equation for the temperature. This function describes how the latent heat is released inside the interface, and should therefore satisfy $h(0) = 0$ and $h(1) = 1$. If $h(\phi) \neq g(\phi)$, the model is no longer variational; however, it has been shown in [33] that more efficient models can be obtained with this additional freedom. In Eq. (44), $h(\phi) = \phi$.
3. Change variables from ϕ to $\psi = (1 + \phi)/2$ and from T to the dimensionless field u. Divide the equation for the phase field by the constant H contained in $f_{\rm int}$, define the phase-field relaxation time by

$\tau = 1/(\Gamma H)$, and combine all constants and numerical prefactors in the last term on the right-hand side in the parameter λ. The expression for λ that results from these steps is identical to Eq. (45). This shows that the Gibbs-Thomson effect is naturally present in the phase-field model through its thermodynamic construction.

5.2. Anisotropy and dendritic growth

All equations discussed so far have been *isotropic*. It is clear that such equations cannot describe the phenomenon of dendritic growth, since a dendrite has well-defined privileged growth directions that are set by the crystallographic axes of the solid. According to microscopic solvability theory, two different effects linked to the crystallographic structure have a decisive influence on the selection of the dendrite operating state: the anisotropies of the interface free energy and of the interface mobility.

The static (capillary) anisotropy leads to a dependence of the interface free energy on the interface orientation. The coordinate system is attached to the crystallographic axes of the growing monocrystal, and the surface free energy is expressed as a function of the interface normal $\hat{n}$ as

$$\gamma(\hat{n}) = \bar{\gamma} a_c(\hat{n}), \tag{56}$$

where $\bar{\gamma}$ is the mean surface free energy and $a_c(\hat{n})$ is a dimensionless function. Similarly, the interface mobility μ_k, or equivalently the kinetic coefficient β of Eq. (42), may depend on the orientation as

$$\beta(\hat{n}) = \bar{\beta} a_k(\hat{n}). \tag{57}$$

These anisotropies lead to a modification of the Gibbs-Thomson boundary condition in the sharp-interface problem. Equation (42) is replaced by

$$u_{\mathrm{int}} = -d_0 \sum_{i=1,2} \left[a_c(\hat{n}) + \frac{\partial^2 a_c(\hat{n})}{\partial \theta_i^2} \right] \frac{1}{R_i} - \beta(\hat{n}) V_n, \tag{58}$$

where the capillary length d_0 is now evaluated using the mean surface free energy $\bar{\gamma}$, R_i are the local principal radii of curvature of the interface, and θ_i are derivatives with respect to the angle along the corresponding principal directions. The new terms arise from the fact that now the interface energy can change in two ways: by a change in the surface area or by a rotation with respect to the crystallographic axes.

Since the phase-field methodology is based on a free energy functional, it is straightforward to incorporate capillary anisotropy by letting the surface free energy contribution f_{int} in Eq. (47) depend on the interface orientation. In view of the general scaling relation for the surface free energy given by Eq. (23), there are several possibilities to achieve this. Historically, the first idea was to make the coefficient of the square gradient term depend on orientation [47, 48, 49]. In the formalism of Eq. (30) (dimensionless free energy density), it is sufficient to replace W by

$$W(\hat{n}) = \bar{W} a_c(\hat{n}). \tag{59}$$

The kinetic anisotropy can then be incorporated by choosing the orientation-dependent phase-field relaxation time by Eq. (46), which remains valid for anisotropic interfaces if W is replaced by its orientation-dependent value [33].

This method works well for weak anisotropy. However, Eq. (59) implies that there is also a variation of the interface thickness with orientation, which may lead to numerical problems for strong anisotropy. This can be avoided by using the formulation of Eq. (31), which directly makes γ and ξ appear in the free energy functional, and by replacing γ by $\gamma(\hat{n})$ at constant ξ. This form of the functional was found to perform well for strong anisotropy [50].

In both cases, the equation for the phase field has to be modified. The correct equation is "automatically" generated by the evaluation of the functional derivative. For a free energy of the form $\mathcal{F} = \int_V f(\phi, \vec{\nabla}\phi)$, where $f(\phi, \vec{\nabla}\phi)$ is the total free energy density (with local and square gradient terms), the general formula for the functional derivative is

$$\frac{\delta \mathcal{F}}{\delta \phi} = \frac{\partial f}{\partial \phi} - \sum_{i=1}^{d} \frac{\partial}{\partial x_i} \frac{\partial f}{\partial (\partial_i \phi)}, \tag{60}$$

where d is the dimension of space, x_i are the (Cartesian) coordinates, and $\partial_i \phi$ denotes the ith component of $\vec{\nabla}\phi$. The outward unit normal vector is expressed in terms of the phase field as

$$\hat{n} = -\frac{\vec{\nabla}\phi}{|\vec{\nabla}\phi|}. \tag{61}$$

Since a_c is a function of $\hat{n}$ and thus of $\vec{\nabla}\phi$, the derivatives of the free energy density with respect to the gradient components make appear the derivatives

of a_c with respect to the orientation that are present in Eq. (58). This straightforward incorporation of surface energy anisotropy is one of the major advantages of the phase-field model with respect to sharp-interface methods. Indeed, the curvatures, directions, and angles that appear in Eq. (58) are contained in the functional derivative of the phase field and do not need to be evaluated explicitly.

The anisotropy function that has been most extensively used is the "standard" cubic anisotropy given by

$$a_c(\hat{n}) = 1 + \epsilon_c[4(n_x^4 + n_y^4 + n_z^4) - 3], \tag{62}$$

where ϵ_c is the anisotropy strength; an equivalent expression holds for the kinetic anisotropy. In two dimensions, the interface orientation is described by a single angle θ, with $\hat{n} = (\cos\theta, \sin\theta)$, and we have simply $\gamma(\theta) = \bar{\gamma}[1 + \epsilon_4 \cos(4\theta)]$. Simulations of dendritic growth have been carried out using this form of the anisotropy, and the results are in good agreement with solvability theory both at high [52, 33] and low undercooling [53]. An example for such a dendrite is shown in Fig. 5. Good agreement with experiments has also been achieved corcerning the anisotropic shape of the dendrite tip at low undercooling [54, 53] and the growth velocity of Nickel dendrites at high undercooling [55]. This proves that a quantitative description of dendritic growth in a pure sustance can be obtained with the help of the phase-field method.

It should also be mentioned that for anisotropies that are strong enough to generate *forbidden orientations*, the phase-field model has to be amended. Indeed, in this situation, there exist orientations in which an interface is unstable with respect to the formation of hill-and-valley structures [56]; for interfaces in these orientations, the equations outlined above become ill-posed, and the model has to be regularized, either by a "convexification" of the anisotropy function [57] or by the addition of higher-order derivatives (such as the square of the Laplacian, or the square of the local interface curvature) in the free-energy functional. See [50] for a more detailed discussion of these issues and the various models that have been proposed.

5.3. Binary alloy

Alloy solidification is obviously of great practical importance. Whereas "real" alloys used in metallurgy have usually multiple components, binary alloys offer the simplest setting in which to develop the methods that can

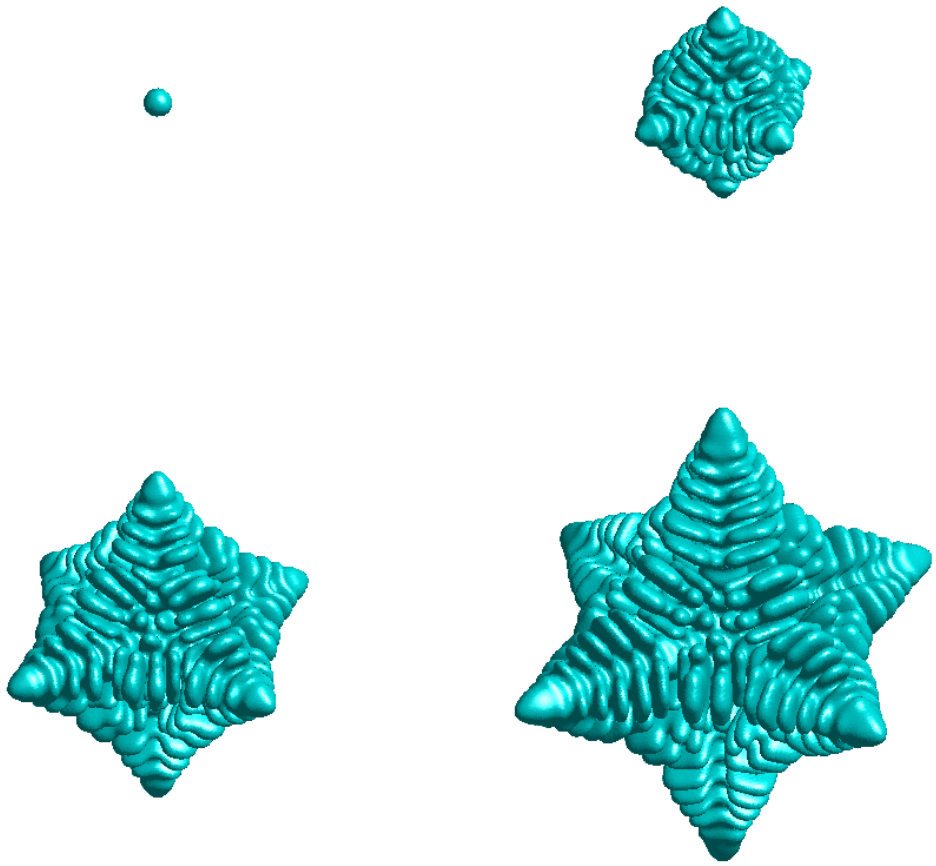

Figure 5: Growth of a dendrite simulated with the anisotropic version of the phase-field model for a pure substance, given by Eqs. (43) and (44), with an anisotropy of the surface free energy given by Eq. (62) with $\epsilon_c = 0.00625$, and isotropic (vanishing) kinetics ($\beta(\hat{n}) = 0$). The dimensionless undercooling is $\Delta = 0.1$, that is, the initial and boundary values of $u = -0.1$. The simulation is carried out with the multi-scale algorithm described in Ref. [51].

later be extended to multi-component systems. Therefore, let us come back to the model system of a binary alloy, which is assumed to have constant total number density ρ (or, equivalently, constant molar volume). The new variable with respect to the pure substance is the composition $c = \rho_B/\rho$.

The earliest attemps to formulate models for binary alloys just extended the formalism for a pure substance presented above (to be more precise, they were not exactly formuated as presented below, but they can easily be brought into this form) [58, 59]. The free energy densities f_s and f_l of the functional given by Eq. (47) are now functions of both T and c, and the equation of motion for the variable c (a conserved quantity) is obtained by the standard procedure,

$$\partial_t c = -\vec{\nabla} \cdot \vec{J} = \vec{\nabla} \cdot \left(M \frac{\delta \mathcal{F}}{\delta c} \right). \tag{63}$$

While this model is a viable representation of the physical system if the thickness of the phase-field interface has its natural (atomistic) width, it is difficult to use it with "upscaled" interfaces. The reason is that the interface properties intrinsically depend on the bulk thermodynamics in this model. This can be understood in several manners. As already found in Eq. (34) in Sec. 3, equilibrium between solid and liquid in a mixture implies that the function $\omega_\nu = f_\nu - \tilde{\mu} c_\nu$ takes the same values ω_{eq} for liquid and solid ($\nu = l, s$). Since the composition of solid and liquid in an alloy differ, this implies that there are two extensive quantities (f and c) which vary across the interface, in addition to the phase field ϕ. If Gibbs dividing surfaces are constructed by the condition of zero interface excesses for c, ϕ, and f following the procedure outlined in section 3, the positions of the three surfaces will in general not coincide, which implies that the interface thermodynamics is non-trivial [34]. The profiles of ϕ and c at equilibrium are actually related, because the condition that the diffusion current vanishes yields

$$\frac{\delta \mathcal{F}}{\delta c} = g(\phi) \frac{\partial f_s}{\partial c} + (1 - g(\phi)) \frac{\partial f_l}{\partial c} = \tilde{\mu}_{\mathrm{eq}} = \mathrm{const.} \tag{64}$$

This equation relates c and ϕ, and at a given point x within the interface, $g(\phi(x)) f_s(c(x)) + (1 - g(\phi(x))) f_l(c(x)) - \tilde{\mu} c(x)$ generally differs from ω_{eq}. According to Eq. (35), this gives a contribution to the interface excess free energy γ. This fact was detected for the first time in Ref. [60].

Another way to reach the same insight is to write down the equilibrium

condition for the phase field across a planar interface. It reads

$$0 = -\frac{\delta \mathcal{F}}{\delta \phi} = K\partial_{xx}\phi - H f'_{\mathrm{dw}}(\phi) + g'(\phi)[f_s(c,T) - f_l(c,T)]. \tag{65}$$

For a pure substance, the free energy densities of solid and liquid are equal; this is not the case for alloys. Therefore, in the interface (where $g'(\phi) \neq 0$) a driving force acts on the phase field that competes with the terms proportional to K and H to shape the interface profile. As a consequence, the surface free energy does not follow the simple scaling of Eq. (23), but also depends on the choice of the bulk free energies.

Different solutions have been developed to overcome this problem and to develop models in which the interface width can be more easily adjusted. The first idea was to start from a "phase-superposition" picture that is based on the general principles of volume-averaged transport equations for multiphase systems [61]. Solid and liquid are seen as two independent macroscopic phases, with two separate composition fields c_s and c_l, which overlap in the diffuse interface region. Since there is, in reality, only one global composition, the additional degree of freedom has to be removed by a supplementary condition. In the case of a dilute binary alloy, one may use the partition relation $c_s = kc_l$, where the partition coefficient k is a constant. With the help of this relation, c_s can be eliminated and the model can be completely written in terms of c_l [62, 43]. In the general case, the relation between the two compositions results from the equilibrium between the solid and liquid pases,

$$\tilde{\mu}_s = \left.\frac{\partial f_s(c,T)}{\partial c}\right|_{c_s} = \tilde{\mu}_l = \left.\frac{\partial f_l(c,T)}{\partial c}\right|_{c_l}. \tag{66}$$

The "true" composition is then obtained as

$$c = c_s g(\phi) + c_l[1 - g(\phi)] = c_l[1 - (1-k)g(\phi)], \tag{67}$$

where the second equality is valid only for a dilute alloy. It is immediately clear that with this convention the combination $f - \tilde{\mu}c$ is a constant through the interface, and thus there is no interface excess energy associated with bulk thermodynamics. The equations of motion for the composition and the phase field are given in [60]; the combination $f - \tilde{\mu}c$ appears as the thermodynamic driving force for the phase field.

A completely equivalent formulation of this model can be given, in which the connection to the model for a pure substance is more straighforward [63].

It starts from the functional

$$\Omega = \int_V \omega_{\text{int}} + \omega_s(\tilde{\mu}, T)g(\phi) + \omega_l(\tilde{\mu}, T)[1 - g(\phi)]. \tag{68}$$

Here, ω_{int} has the same form as f_{int}, and $\omega_\nu = f_\nu - \tilde{\mu}c$ are Legendre transforms of the free energy densities, which means that they depend on the diffusion potential instead of the composition. This functional has been called "grand potential functional", although the correct expression for the grand potential of a binary mixture is $f - \mu_A\rho_A - \mu_B\rho_B$; however, in the case of constant molar volume, the function ω satisfies exactly the same thermodynamic relations as the grand potential of a pure substance if the chemical potential is replaced by the diffusion potential. In particular,

$$\frac{\partial \omega_\nu}{\partial \tilde{\mu}} = -c_\nu. \tag{69}$$

The equations of motion for the variables ϕ and $\tilde{\mu}$ can now be obtained in a straightforward way. The equilibrium equation for the phase field is equivalent to Eq. (65), with the difference $f_s - f_l$ replaced by $\omega_s - \omega_l$. Since the latter is zero at equilibrium, the interface profile is determined by ω_{int} alone, and the scaling of Eq. (23) applies, as desired.

The variation of Ω with respect to $\tilde{\mu}$ yields an espression for the local composition,

$$\frac{\delta\Omega}{\delta\tilde{\mu}} = \frac{\partial\omega_s}{\partial\tilde{\mu}}g(\phi) + \frac{\partial\omega_l}{\partial\tilde{\mu}}[1 - g(\phi)] = -c(\tilde{\mu}, \phi). \tag{70}$$

It can easily be seen using Eq. (69) that this expression is actually identical to Eq. (67). By taking the time derivative of $c(\tilde{\mu}, \phi)$ and using mass conservation, $\partial_t c = \vec{\nabla}(M\vec{\nabla}\tilde{\mu})$, one obtains an equation for the diffusion potential,

$$\chi(\tilde{\mu}, T, \phi)\partial_t\tilde{\mu} = \vec{\nabla}(M\vec{\nabla}\tilde{\mu}) + (c_l - c_s)g'(\phi)\partial_t\phi, \tag{71}$$

with

$$\chi(\tilde{\mu}, T, \phi) = \chi_s(\tilde{\mu}, T)g(\phi) + \chi_l(\tilde{\mu}, T)[1 - g(\phi)] \qquad \chi_\nu = \frac{\partial^2\omega_\nu}{\partial\tilde{\mu}^2} \tag{72}$$

being a generalized susceptibility [5]. The structure of this equation is perfectly equivalent to the one of Eq. (53) for the temperature, with χ playing

the role of the specific heat C, and $c_l - c_s$ in place of $s_l - s_s$. Of course, this just expresses the thermodynamic equivalence of the intensive variables T and $\tilde{\mu}$ and the extensive variables s and c. The major difference, however, with the case of a pure substance is that χ is generally quite different for liquid and solid, so that the dependence of χ on ϕ cannot be neglected.

5.4. Antitrapping current

The model outlined above, as well as the models of Refs. [60, 43] are still not suitable for the quantitative modelling of solidification microstructures with upscaled interfaces. The reason is the phenomenon of *solute trapping*, which occurs during the solidification of alloys at sufficiently high velocity. Since liquid and solid have different compositions, the composition of a piece of matter has to change during the solidification process; some components are rejected into the liquid, others are incorporated into the solid. Generally, solute (impurities) has to be rejected during solidification. When the driving force for solidification (provided, for example, by rapid cooling) is high, the interface advances at such a high velocity that these redistribution processes cannot be completed, and the solid remains at a composition that differs from the equilibrium one. As a simple criterion for the occurrence of solute trapping, one may compare the time that an interface needs to propagate by a distance equal to its intrinsic thickness, ξ/V, to the characteristic time of diffusion through the same interface, ξ^2/D, where D is the solute diffusivity within the interface. If the ratio of the two, $\xi V/D$, is much smaller than unity, the solute atoms have enough time to escape from the advancing solid; in the opposite limit, they are *trapped*. This means that the solid does not grow at the composition that corresponds to the thermodynamic equilibrium with the liquid, but at a higher solute content. In other words, the diffusion potential does not have the same value at the two sides of the interface: there is a jump in this intensive quantity across the interface.

Although, under such circumstances, the hypothesis that local equilibrium is established on the scale of a coarse-graining cell breaks down (recall that we had supposed that intensive quantities are constant within a cell, which is not the case any more for the diffusion potential), phase-field models can describe solute trapping quite well [64]: the transition from growth in local equilibrium to complete solute trapping with increasing growth velocity is well reproduced when the parameter $\xi V/D$ is varied. The problem for quantitative simulations is now obvious: since this effect depends on the

thickness of the interface, its magnitude is greatly exaggerated if the interface thickness is upscaled in simulations. This means that solute trapping will appear for solidification velocities that are much smaller than those for which it is really observed in experiments. For accurate simulations, it has therefore to be eliminated from the model.

A way to accomplish this was developed in Ref. [65] for isothermal solidification, and in Ref. [46] for directional solidification: an *antitrapping current* is added to the model. This is an additional contribution to the solute current which counteracts solute trapping. For this purpose, it should be proportional to the interface thickness and to the growth velocity, and it should be directed from the solid to the liquid in order to assist solute redistribution. Concretely, the solute current is written as

$$\vec{J} = -M\vec{\nabla}\tilde{\mu} + \vec{J}_{\mathrm{at}}, \tag{73}$$

with the antitrapping current

$$\vec{J}_{\mathrm{at}} = -a(\phi)(c_l - c_s)\xi\partial_t\phi\hat{n}, \tag{74}$$

where $a(\phi)$ is a dimensionless function of ϕ that depends on the details of the model, and $c_l - c_s$ is the composition jump between the phases, taken at equilibrium. For the models of Refs. [65, 46] that describe the solidification of binary alloys, the function $a(\phi)$ is actually just a constant, the value of which has to be determined by matched asymptotic expansions. The details of this procedure can be found in Ref. [46].

These works were the first examples for a successful interface upscaling in phase-field modelling of alloy solidification; since then, this methodology has been used to explore dendritic and cellular solidification, and convincing quantitative agreement between simulations, theories, and experiments has been achieved [66, 67, 68, 69]. The antitrapping methodology has also been extended to other alloy models [70, 13, 63, 23]. Furthermore, the models for pure substance and alloy have been combined to build a model for crystal growth limited simultaneously by heat and solute diffusion [71], which has then been used to explore dendritic growth in this regime [72].

5.5. Multi-phase and multi-component solidification

Many solidification phenomena involve multiple phases. The simplest example is the solidification of eutectic alloys, during which two different solids with distinct compositions are formed from the liquid. For such situations,

models with more than one order parameter are needed in order to distinguish between phases. In the earliest attempts to formulate such models, one phase field and the composition field [73, 74] or two phase fields [75] were used, with free energies in the form of simple Landau expansions. While these models were capable of describing the basic features of eutectic growth, their generalization to different alloy phase diagrams or a larger number of phases is not straightforward.

A general approach was provided by the *multi-phase-field method*, first introduced in Ref. [76]. One phase field is associated to each thermodynamic phase that is present in the system, and interpreted as local volume fraction, which implies

$$\sum_{\nu=1}^{N} \phi_i(\vec{x}) = 1 \qquad \forall\ \vec{x} \tag{75}$$

for N phases. With this constraint, there are obviously only $N-1$ independent fields, and one variable could immediately be eliminated. However, it is advantageous to keep all the degrees of freedom for the formulation of the free energy functional, because this gives rise to particularly simple and symmetric functional forms. The constraint can be taken into account at the end with the help of a Langrange multiplier.

A multi-phase system contains multiple types of interfaces, and therefore a generalization of the interface free energy density f_{int} is needed in terms of the multiple phase fields. The extensions of the square gradient terms that are most commonly used are $\sum_{\alpha\beta} K_{\alpha\beta} \vec{\nabla}\phi_\alpha \cdot \vec{\nabla}\phi_\beta$ or $\sum_{\alpha\beta} K_{\alpha\beta} |q_{\alpha\beta}|^2$ with $q_{\alpha\beta} = \phi_\alpha \vec{\nabla}\phi_\beta - \phi_\beta \vec{\nabla}\phi_\alpha$. Both expressions are sums over pairwise terms that are zero everywhere except in α-β interfaces or multi-junctions. For the local free energy density, we need a multi-well potential function over the $N-1$-dimensional state space of the phase field configurations (taking into account the sum constraint), with N distinct minima that describe the possible phases.

The choice of the gradient terms and the potential function presents some new non-trivial issues that are illustrated in Fig. 6 for the case of three phases. The state space for the three phase fields, taking into account the sum constraint, can be conveniently visualized in the standard simplex, an equilateral triangle in which each corner represents a pure phase (one of the fields equals 1, all others 0). The free energy density must have a minimum on each corner to generate the correct number of phases, with potential barriers in between (for an example, see Fig. 7). Interfaces between phases

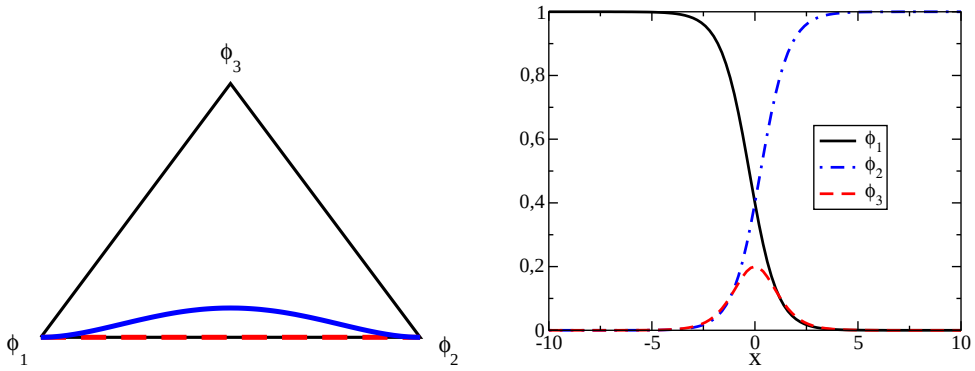

Figure 6: Left: representation of the state space of a multi-phase-field model with three phases ($\phi_1 + \phi_2 + \phi_3 = 1$) in a simplex. Each corner corresponds to a pure phase. The two lines represent different interfaces between phases 1 and 2. Along the red dashed line, $\phi_1 + \phi_2 = 1$. Along the full blue line, the phase fields vary as depicted in the graph to the right for an interface along the x direction.

correspond to trajectories in the state space that go from one minimum to another. The properties of the interface are determined by this trajectory, which is influenced both by the shape of the potential landscape and the gradient terms (see Ref. [77] for a detailed illustration and discussion of this point in a specific model).

Since a precise control of the interface properties is mandatory for interface upscaling, one would like, in particular, to have "clean" two-phase interfaces. That is, in a system in which only bulk phases α and β are present, the interface between these phases should be free of the presence of any other phase, that is, one requires to have $\phi_\alpha + \phi_\beta = 1$ instead of Eq. (75). In the simplex of Fig. 6, this corresponds to a perfectly straight line along one of the edges (the dashed red line). In contrast, if the trajectory travels inside the simplex (full blue line), this corresponds to the presence of additional phases inside the interface, and thus to "third-phase adsorption". This phenomenon (which could be present in real systems) makes the analytic solution of interface equations and the calculations of asymptotic matching impossible. For a quantitative modelling of solidification, the presence of such additional phases in the interfaces must therefore be avoided.

For a smooth free-energy functional, this requirement imposes non-trivial conditions on the potential landscape and the gradient terms. A formulation that allows for a complete control of the interface properties in three-phase systems (for example, one liquid and two solids) has been given in

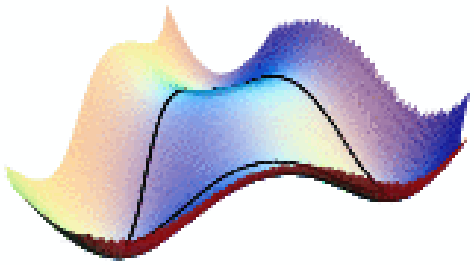

Figure 7: Triple-well potential of the three-phase model detailed in [78], plotted over the three-phase simplex (black lines). This multi-well potential, $\sum_{i=1}^{3}[\phi_i^2(1-\phi_i)^2]$, generates interfaces that run along the edges of the simplex.

Ref. [78] and extensively benchmarked against sharp-interface models and experiments [79]. The potential landscape is shown in Fig. 7, plotted over the three-phase simplex. Unfortunately, a generalization of this approach to more than three phases is not straightforward. This task is simplified by the use of the *multi-obstacle potential*. In the "double-obstacle potential", the double-well function for a simple phase field, $f_{\mathrm{dw}}(\phi)$, is replaced by

$$f_{\mathrm{do}}(\phi) = \begin{cases} H\phi(1-\phi) & \text{if } 0 < \phi < 1 \\ \infty & \text{otherwise} \end{cases} \tag{76}$$

which can be seen as the limit of zero temperature of Eq. (8). In practice, when the simulation code yields a value of the phase field lower than 0 or larger than 1, ϕ is just set back to the limit of the allowed interval with the help of an "if" instruction. The advantage of this formulation is that it yields an evolution equation for ϕ that is linear and has as equilibrium solution a simple sine profile. Moreover, since the derivative of the potential at the (cusp-like) minima is finite, there is always a finite force that drives the phase field to its bulk values. For multiple phase fields, the configuration space is restricted to the simplex defined by $\phi_\nu > 0 \ \forall \ \nu$, $\sum_\nu \phi_\nu \leq 1$. The finite slope of the potential landscape at the borders of this simplex "pushes" the interface solution against the "walls" (obstacles), which provides the desired "clean" interfaces. In summary, a simple version of the interface energy can be written as

$$f_{\mathrm{int}} = \sum_{\alpha,\beta=1}^{N} [K_{\alpha\beta}\vec{\nabla}\phi_\alpha \cdot \vec{\nabla}\phi_\beta + H_{\alpha\beta}\phi_\alpha(1-\phi_\beta)]. \tag{77}$$

The surface free energy for each interface can then be controlled as in the case of a single phase field with the help of the constants $K_{\alpha\beta}$ and $H_{\alpha\beta}$. If these values are strongly different for different interfaces, higher-order terms (products of more than two phase fields) may need to be added in order to avoid third-phase adsorption.

The free energy functional is completed by the thermodynamic part, that is, the contribution of the bulk phases. This is straightforward: since each phase ν occupies a certain spatial domain described by a specific phase field ϕ_ν, the indicator function is approximated by $g(\phi_\nu)$, and the bulk contribution to the free energy is written as

$$f_{\text{bulk}} = \sum_{\nu=1}^{N} g(\phi_\nu) f_\nu(c, T). \tag{78}$$

One can see that Eq. (47) is a special case of this expression for two phases. Also, it is clear that in order to obtain a model with good upscaling properties, either the phase-superposition approach has to be generalized to multiple phases (with the introduction of a separate composition field for each phase) [62], or a grand-canonical approach has to be used [23].

Let us now come to the equation of motion for the multiple phase fields. Since the phase fields can still be seen as non-conserved order parameters, they should obey the relaxation dynamics of Eq. (11). If one such equation is written down for each field, only $N-1$ mobility coefficients can be specified, whereas there are in total $N(N-1)/2$ different types of interfaces in an N-phase system (the number of possibilities to choose two different phases out of N). At a first glance, it therefore seems that the kinetic properties of each interface cannot be controlled separately. However, there are several possibilities to cirvumvent this difficulty. Either, the evolution equation can be made non-linear by making the mobilities depend on the phase fields, which gives the possibility to give the mobility the desired value on each interface [78]. Or, the principles of out-of-equilibrium thermodynamics may be used, which stipulate that the time evolution of any state variable can depend on *all* the thermodynamic driving forces in the system. Therefore, the general evolution equation for the phase fields reads

$$\partial_t \phi_\alpha = -\sum_{\beta=1}^{N} \Gamma_{\alpha\beta} \frac{\delta \mathcal{F}}{\delta \phi_\beta}. \tag{79}$$

Furthermore, the Onsager symmetry principles imply that $\Gamma_{\alpha\beta} = \Gamma_{\beta\alpha}$. Since there are only $N-1$ independent fields, there are only $N(N-1)/2$ independent coefficients in the matrix $\Gamma_{\alpha\beta}$, which precisely corresponds to the number of independent interfaces. A particularly intuitive manner of rewriting the above equation is

$$\partial_t \phi_\alpha = \sum_{\beta \neq \alpha} \tilde{\Gamma}_{\alpha\beta} \left(\frac{\delta \mathcal{F}}{\delta \phi_\beta} - \frac{\delta \mathcal{F}}{\delta \phi_\alpha} \right). \tag{80}$$

In this form, the rate of transformation of phase α is decomposed in the same manner as for a network of chemical reactions, in which a substance α can transform into various other chemcials by different reaction pathways. The coefficients $\tilde{\Gamma}_{\alpha\beta}$ directly control the rate of transformation from phase α to β, and therefore the kinetics of the $\alpha\beta$ interfaces.

Let us finally briefly touch upon the subject of multi-component systems, which is a whole area of research in itself; here, only the aspects that are important for the construction of phase-field models will be very briefly mentioned. In a system with a total number of K components, the composition fields c_i give the molar fractions of component i and satisfy

$$\sum_{i=1}^{K} c_i = 1. \tag{81}$$

It is customary to designate one of the components (in principle, the majority component, say component K) as the "solvent", and to eliminate its composition field to obtain $K-1$ independent variables. The conjugate intensive variables are the $K-1$ diffusion potentials $\tilde{\mu}_i = (\mu_i - \mu_K)/V_a$, where μ_i are the chemical potentials and V_a the atomic volume. The diffusion current of component i is then written as

$$\vec{J}_i = -\sum_{j=1}^{K-1} M_{ij} \vec{\nabla} \tilde{\mu}_j \tag{82}$$

with a matrix of mobility coefficients M_{ij}. Each component obeys a separate conservation law,

$$\partial_t c_i = -\vec{\nabla} \cdot \vec{J}_i. \tag{83}$$

The driving force for phase transformations that appears in the equation of motion for the phase fields has also to be generalized. It now involves the

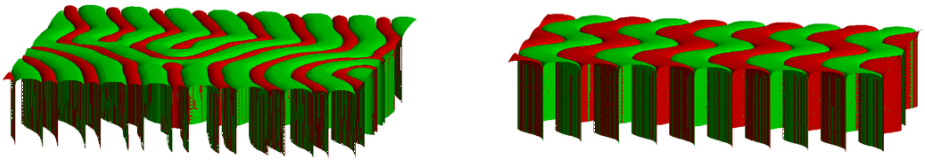

Figure 8: Simulations of eutectic microstructures, carried out with the multi-phase-field model of Ref. [78]. The solid grows upward in a temperature gradient, and the liquid (transparent) solidifies into two solid phases. Disordered labyriths (left) and zig-zag structures have been obtained [81], in good agreement with experimental observations [82].

difference between the functions

$$\omega_\nu = f_\nu - \sum_{i=1}^{K-1} \tilde{\mu}_i c_i \tag{84}$$

taken for two phases α and β. The evolution equation for the phase fields can be written down either in the phase-superposition approach, in which the driving force is evaluated in terms of separate concentration fields for each phase and component [80, 13], or in the grand-canonical approach, in which the functions ω are used to construct a generalization of the functional Ω of Eq. (68), and a change of variables from the compositions c_i to the diffusion potentials $\tilde{\mu}_i$ is made [23]. Several generalizations of the antitrapping current to multi-phase and multi-component systems have also been proposed [78, 70, 13, 23]. Therefore, in principle, all the elements needed for a quantitative modelling of solidification in multi-component and multi-phase systems are available.

As an example for the use of multi-phase-field models, Fig. 8 shows simulations of microstructures obtained during the directional solidification of a binary eutectic alloy. In such an alloy, a liquid of composition close to the eutectic point can solidify in two different solids of distinct compositions, and the solidification process generally results in a composite in which the crystals of the two phases are intertwined in complex patterns. The two most frequent morphologies are regular lamellae and rods, but more complicated patterns have recently been observed in real-time *in situ* observations of transparent eutectic alloys [82], among which disordered labyrinths and zig-zag patterns, which are both well reproduced by the model [81].

6. Conclusions and open questions

The models described in this chapter represent developments that have spanned more than three decades. During this period, enormous progress has been made both in model development and in the understanding of the solidification phenomena that have been studied with their help. Nevertheless, there is still a large number of open questions. I have not touched at all the coupling of phase-field models to mechanics (both hydrodynamics and elasticity), which could be the subject of a review on its own, and which presents important and exciting research opportunities. I will conclude this chapter by commenting on some active and open research questions in diffusion-limited crystal growth, within the areas that are covered in the preceding sections.

- Asymptotics. The asymptotic matching described in Sec. 4 has made it possible to perform accurate and efficient simulations in two important special cases: the symmetric model (equal diffusivities in both phases), and the one-sided model (no diffusion in the solid). There is, presently, no generalization for arbitrary diffusion coefficients in the two phases. Attemps have been made to formulate such models by generalizing the antitrapping concept [13, 83], but these models work only well in cases in which the current arriving at the interface is zero (or at least small) in one of the phases [22]. In the general case, there always remain some thin-interface corrections that make an accurate interface upscaling impossible. A solution to this problem would be of great interest.

- Anisotropy. Surprising results have recently been obtained when the effect of interface anisotropy was explored with functional forms that go beyond the simple expressions given by Eq. (62). For instance, "hyperbranched" dendrites can be obtained by combining two different cubic harmonics [84]; a "dendrite-orientation transition" is also observed in alloys of substances that have different crystal structures [85]. Finally, anisotropy effects play also an important role for the selection of cellular microstructures [67]. All these results show that there is a lot left to understand concerning the relation between anisotropy and structure selection.

- Junctions. In multi-phase-field models, trijunctions, triple lines, and multi-junctions naturally appear. The equilibrium properties of these

singularities conform to the well-known Young-Laplace law, which is implied by the thermodynamic construction of the model. However, much remains to be learned about non-equilibrium behavior. It has already been shown [78] that the dynamics of trijunctions in phase-field models is slightly different from the assumtions usually made in sharp-interface models. Moreover, the energetics of such junctions can be controlled in phase-field models by adding suitable higher-order terms (products of three or more phase fields) to the free-energy functional. This possibility has been explored little so far.

- Growth and diffusion kinetics. Up to now, attention has been mostly focused on models that permit to maintain local equilibrium at the interfaces. However, in many cases, it is necessary to introduce strong interface kinetics or departure from equilibrium between the two sides of an interface in a well-controlled way, for example if slowly diffusing species are present in multi-component systems. In a recent line of works, several authors have formulated phase-field models that contain new coupling terms between the phase-field and the diffusion equation [86, 87, 88], which lead to discontinuities in intensive fields at the interface. This approach also yields an interesting new derivation of the antitrapping current. Moreover, the "phase-superposition" approach has been generalized, replacing the equilibrium condition of Eq. (66) between the phases by a kinetic equation for the individual phase compositions [89, 90]. Both of these approaches could considerably extend the domain of applicability of phase-field models and should be further pursued.

- Polycrystals. Monocrystals are actually quite rare in nature; most crystal growth processes lead to the spontaneous emergence of *polycrystals*, that is, solids that consists of multiple grains of the same thermodynamics phase, separated by grain boundaries. Two very different phase-field approaches have been pursued to model polycrystals. The first is an application of the multi-phase-field concept: each grain in represented by a different phase field, but with identical free energy densities [91, 92, 77]. The second is the orientation-field approach, in which a single phase field is combined with an orientation field that indicates the local direction of the crystallographic axes. Whereas the validity of the evolution equation for the orientation can actually be

questioned [22], these models were successful in describing a large variety of polycrystalline growth structures [93, 94]. It is highly interesting from a conceptual point of view to further explore the possibilities of such models and their eventual relation to crystal plasticity.

- Multi-component systems. As already mentioned, several models have been proposed and used for multi-component and multi-phase systems. They differ in various choices for the free energy functionals, the interpolation schemes, and the mobility functions. Only in very few cases have rigorous asymptotics been carried out. Therefore, there is still a need for comprehensive benchmarking in order to thoroughly assess their reliability. This task is made difficult by the fact that multi-component multi-phase systems are inherently complex, and thus the definition of useful and accessible benchmark problems is far from simple. However, the large practical impact of such modelling tools is expected to provide an important driving force for future developments in this area.

References

[1] J. Stefan, Sitzungsberichte der Österreichischen Akademie der Wissenschaften Mathematisch-Naturwissenschaftliche Klasse, Abteilung 2, Mathematik, Astronomie, Physik, Meteorologie und Technik 98 (1889) 965–983.

[2] J. Stefan, Annalen der Physik und Chemie 42 (1891) 269–286.

[3] L.-Q. Chen, Annu. Rev. Mater. Res. 32 (2002) 113.

[4] D. M. Anderson, G. B. McFadden, A. A. Wheeler, Annual Review of Fluid Mechanics 30 (1998) 139.

[5] J. S. Langer, in: C. Godrèche (Ed.), Solids far from equilibrium, Edition Aléa Saclay, Cambridge University Press, Cambridge, UK, 1991, pp. 297–363.

[6] W. J. Boettinger, J. A. Warren, C. Beckermann, A. Karma, Annu. Rev. Mater. Res. 32 (2002) 163–194.

[7] M. Plapp, in: M. Wang, K. Tsukamoto, D. Wu (Eds.), Selected topics on crystal growth - 14th International Summer School on Crystal Growth, AIP Conference Proceedings Vol. 1270, Melville, 2010, pp. 247–254.

[8] M. Plapp, in: R. Mauri (Ed.), Multiphase microfluidics: The Diffuse Interface Model, Springer, Wien, 2012, pp. 129–175.

[9] N. Provatas, K. Elder, Phase-field methods in materials science and engineering, Wiley-VCH, Weinheim, 2010.

[10] M. Plapp, J. Cryst. Growth 303 (2007) 49–57.

[11] I. Singer-Loginova, H. M. Singer, Rep. Prog. Phys. 71 (2008) 106501.

[12] H. Emmerich, Adv. Phys. 57 (2008) 1–87.

[13] I. Steinbach, Model. Simul. Mater. Sci. Eng. 17 (2009) 073001.

[14] I. Steinbach, Annu. Rev. Mater. Res. 43 (2013) 89–107.

[15] J. S. Langer, Rev. Mod. Phys. 52 (1980) 1.

[16] W. Kurz, D. J. Fisher, Fundamentals of Solidification, Trans Tech Publications, Zurich, Switzerland, 1998.

[17] J. A. Dantzig, M. Rappaz, Solidification, EPFL Press, Lausanne, 2009.

[18] J. S. Rowlinson, J. Stat. Phys. 20 (1979) 197–244.

[19] J. W. Cahn, J. E. Hilliard, J. Chem. Phys. 28 (1958) 258–267.

[20] O. Penrose, P. C. Fife, Physica D 43 (1990) 44–62.

[21] M. Conti, Phys. Rev. E 64 (2001) 051601.

[22] M. Plapp, Phil. Mag. 91 (2011) 25–44.

[23] A. Choudhury, B. Nestler, Phys. Rev. E 85 (2012) 021602.

[24] J.-F. Gouyet, M. Plapp, W. Dieterich, P. Maass, Adv. Phys. 52 (2003) 523–638.

[25] Q. Bronchart, Y. L. Bouar, A. Finel, Phys. Rev. Lett. 100 (2008) 015702.

[26] T. Garnier, A. Finel, Y. L. Bouar, M. Nastar, Phys. Rev. B 86 (2012).

[27] A. Karma, W.-J. Rappel, Phys. Rev. E 60 (1999) 3614–3625.

[28] J. J. Hoyt, M. Asta, A. Karma, Mat. Sience Eng. R 41 (2003) 121.

[29] P. C. Hohenberg, B. I. Halperin, Rev. Mod. Phys. 49 (1977) 435–479.

[30] J. S. Langer, in: G. Grinstein, G. Mazenko (Eds.), Directions in Condensed Matter Physics, World Scientific, Singapore, 1986, pp. 165–186.

[31] G. J. Fix, in: A. Fasano, M. Primicerio (Eds.), Free boundary problems: Theory and applications, Piman, Boston, 1983, p. 580.

[32] J. B. Collins, H. Levine, Phys. Rev. B 31 (1985) 6119–6122.

[33] A. Karma, W.-J. Rappel, Phys. Rev. E 57 (1998) 4323–4349.

[34] P. Nozières, in: C. Godrèche (Ed.), Solids far from equilibrium, Edition Aléa Saclay, Cambridge University Press, Cambridge, UK, 1991, pp. 1–154.

[35] J. W. Cahn, in: W. C. Carter, W. C. Johnson (Eds.), The selected works of John W. Cahn, The Minerals, Metals, and Materials Society, Warrendale, 1998, p. 379.

[36] M. R. P. J. Steinhardt, D. R. Nelson, Phys. Rev. B 28 (1983) 784–805.

[37] J. J. Hoyt, M. Asta, A. Karma, Phys. Rev. Lett. 86 (2001) 5530–5533.

[38] T. V. Ramakrishnan, M. Yussouff, Phys. Rev. B 19 (1979) 2775–2794.

[39] K.-A. Wu, A. Karma, J. J. Hoyt, M. Asta, Phys. Rev. B 73 (2006) 094101.

[40] J. A. Sethian, Level Set Methods and Fast Marching Methods : Evolving Interfaces in Computational Geometry, Fluid Mechanics, Computer Vision, and Materials Science, Cambridge University Press, Cambridge, 1999.

[41] P. M. D. Bedeaux, A. M. Albano, Physica A 82 (1976) 438–462.

[42] B. Caroli, C. Caroli, B. Roullet, in: C. Godrèche (Ed.), Solids far from equilibrium, Edition Aléa Saclay, Cambridge University Press, Cambridge, UK, 1991, pp. 155–296.

[43] C. Beckermann, H.-J. Diepers, I. Steinbach, A. Karma, X. Tong, J. Comput. Phys. 154 (1999) 468.

[44] Y. Sun, C. Beckermann, Physica D 198 (2004) 281.

[45] R. F. Almgren, SIAM J. Appl. Math. 59 (1999) 2086–2107.

[46] B. Echebarria, R. Folch, A. Karma, M. Plapp, Phys. Rev. E 70 (2004) 061604.

[47] G. Caginalp, P. Fife, Phys. Rev. B 34 (1986) 4940–4943.

[48] G. B. McFadden, A. A. Wheeler, R. J. Braun, S. R. Coriell, R. F. Sekerka, Phys. Rev. E 48 (1993) 2016–2024.

[49] R. Kobayashi, Physica D 63 (1993) 410–423.

[50] S. Torabi, J. Lowengrub, A. Voigt, S. Wise, Proc. Roy. Soc. A 465 (2009) 1337–1359.

[51] M. Plapp, A. Karma, J. Comput. Phys. 165 (2000) 592.

[52] A. Karma, W.-J. Rappel, J. Cryst. Growth 174 (1997) 54–64. 10th American Conference on Crystal Growth/9th International Conference on Vapor Growth and Epitaxy, VAIL, CO, AUG 04-09, 1996.

[53] A. Karma, Y. H. Lee, M. Plapp, Phys. Rev. E 61 (2000) 3996–4006.

[54] J. C. LaCombe, M. B. Koss, V. E. Fradkov, M. E. Glicksman, Phys. Rev. E 52 (1995) 2778–2786.

[55] J. Bragard, A. Karma, Y. H. Lee, M. Plapp, Interface Science 10 (2002) 121–136.

[56] C. Herring, Phys. Rev. 82 (1951) 87–93.

[57] J. J. Eggleston, G. B. McFadden, P. W. Voorhees, Physica D 150 (2001) 91–103.

[58] A. A. Wheeler, W. J. Boettinger, G. B. McFadden, Phys. Rev. A 45 (1992) 7424–7439.

[59] G. Caginalp, W. Xie, Phys. Rev. E 48 (1993) 1897–1909.

[60] S. G. Kim, W. T. Kim, T. Suzuki, Phys. Rev. E 60 (1999) 7186–7197.

[61] J. Ni, C. Beckermann, Met. Trans. B 22 (1991) 349–361.

[62] J. Tiaden, B. Nestler, H.-J. Diepers, I. Steinbach, Physica D 115 (1998) 73–86.

[63] M. Plapp, Phys. Rev. E 84 (2011) 031601.

[64] N. A. Ahmad, A. A. Wheeler, W. J. Boettinger, G. B. McFadden, Phys. Rev. E 58 (1998) 3436.

[65] A. Karma, Phys. Rev. Lett. 87 (2001) 115701.

[66] M. Greenwood, M. Haataja, N. Provatas, Phys. Rev. Lett. 93 (2004) 246101.

[67] S. Gurevich, A. Karma, M. Plapp, R. Trivedi, Phys. Rev. E 81 (2010) 011603.

[68] B. Echebarria, A. Karma, S. Gurevich, Phys. Rev. E 81 (2010) 021608.

[69] N. Bergeon, D. Tourret, L. Chen, J.-M. Debierre, R. Guérin, A. Ramirez, B. Billia, A. Karma, R. Trivedi, Phys. Rev. Lett. 110 (2013) 226102.

[70] S. G. Kim, Acta Materialia 55 (2007) 4391–4399.

[71] J. C. Ramirez, C. Beckermann, A. Karma, H.-J. Diepers, Phys. Rev. E 69 (2004) 051607.

[72] J. C. Ramirez, C. Beckermann, Acta Mater. 53 (2005) 1721–1736.

[73] A. Karma, Phys. Rev. E 49 (1994) 2245–2250.

[74] K. R. Elder, F. Drolet, J. M. Kosterlitz, M. Grant, Phys. Rev. Lett. 72 (1994) 677–680.

[75] A. A. Wheeler, G. B. McFadden, W. J. Boettinger, Proc. Roy. Soc. A 452 (1996) 495–525.

[76] I. Steinbach, F. Pezzolla, B. Nestler, M. Seeßelberg, R. Prieler, G. J. Schmitz, J. L. L. Rezende, Physica D 94 (1996) 135–147.

[77] N. Moelans, B. Blanpain, P. Wollants, Phys. Rev. B 78 (2008) 024113.

[78] R. Folch, M. Plapp, Phys. Rev. E 72 (2005) 011602.

[79] M. Perrut, A. Parisi, S. Akamatsu, S. Bottin-Rousseau, G. Faivre, M. Plapp, Acta Mat. 58 (2010) 1761–1769.

[80] J. Eiken, B. Böttger, I. Steinbach, Phys. Rev. E 73 (2006) 066122.

[81] A. Parisi, M. Plapp, Acta Materialia 56 (2008) 1348.

[82] S. Akamatsu, S. Bottin-Rousseau, G. Faivre, Phys. Rev. Lett. 93 (2004) 175701.

[83] M. Ohno, K. Matsuura, Phys. Rev. E 79 (2009) 031603.

[84] T. Haxhimali, A. Karma, F. Gonzales, M. Rappaz, Nature Materials 5 (2006) 660–664.

[85] J. A. Dantzig, P. D. Napoli, J. Friedli, M. Rappaz, Met. Mat. Trans. A 44A (2013) 5532–5543.

[86] E. A. Brener, G. Boussinot, Phys. Rev. E 86 (2012).

[87] G. Boussinot, E. A. Brener, Phys. Rev. E 88 (2013).

[88] A. Fang, Y. Mi, Phys. Rev. E 87 (2013).

[89] I. Steinbach, L. Zhang, M. Plapp, Acta Mater. 60 (2012) 2689–2701.

[90] L. Zhang, I. Steinbach, Acta Mater. 60 (2012) 2702–2710.

[91] D. Fan, L.-Q. Chen, Acta Mater. 45 (1997) 611–622.

[92] S. G. Kim, D. I. Kim, W. T. Kim, Y. B. Park, Phys. Rev. E 74 (2006) 061605.

[93] L. Granasy, T. Pusztai, T. Börzsönyi, J. A. Warren, J. F. Douglas, Nature Materials 3 (2004) 645–650.

[94] L. Gránásy, T. Pusztai, G. Tegze, J. A. Warren, J. F. Douglas, Phys. Rev. E 72 (2005) 011605.